

# Cranfield

College of Aeronautics Report 8323

August 1983

TECHNISCHE UNIVERSITEIT DELFT  
LUCHTVAART- EN RUIMTEVAARTTECHNIEK  
BIBLIOTHEEK  
Kluyverweg 1 - 2629 HS DELFT

## Ground Effect on a Rotor Wake

by E.A. BOYD and I. KUSMARWANTO

College of Aeronautics,  
Cranfield Institute of Technology,  
Cranfield, Bedford, U.K.

5 MAART 1984

TECHNISCHE HOGESCHOOL DELFT  
LUCHTVAART- EN RUIMTEVAARTTECHNIEK  
BIBLIOTHEEK  
Kluyverweg 1 - DELFT

# Cranfield

College of Aeronautics Report 8323

August 1983

## Ground Effect on a Rotor Wake

by E.A. BOYD and I. KUSMARWANTO

College of Aeronautics,  
Cranfield Institute of Technology,  
Cranfield, Bedford, U.K.

ISBN 0 902937 93 6

£7.50

*"The views expressed herein are those of the authors alone and do not necessarily represent those of the Institute."*

## Summary

This paper reports an experimental study of the ground effect on a rotor wake when the rotor is operating at a height of less than one rotor diameter above the ground. Particular attention was paid to how the rotor slipstream reacts to the oncoming wind and to the ground vortex generated when the wake eventually strikes the ground.

The rotor wake was visualized by smoke, the ground vortex by a tuft grid and smoke and the ground interaction boundary by a surface flow visualization. An attempt was made to measure the strength of the ground vortex using pitot and static tubes fine enough to cause little disturbance to the vortex field.

Details are given of a new rig planned to extend the reported measurements.

## Contents

Page

Summary

List of Figures

Notation

Introduction

1

### 1. Background

1.1 Rotor wake

2

1.2 Ground effect on a rotor

3

1.3 Ground effect on a rotor wake

3

### 2. Experimental Facilities

2.1 Rotor test rig

5

2.1.1 Rotor test stand

5

2.1.2 Model Rotor

6

2.2 Measuring devices and ancillaries

7

2.3 Photographic equipment

7

2.4 Windtunnel

7

### 3. Experimental Technique

3.1 Flow visualization

8

3.1.1 Smoke visualization

8

3.1.2 Surface flow visualization

9

3.1.3 Tuft grid visualization

9

3.2 Velocity measurement technique

9

3.2.1 Measurement of the tunnel speed

10

3.2.2 Measurement of the vortex

tangential velocity

10

3.2.3 Measurement of vertical velocity

through the disc

10

### 4. Experimental Programme

11

4.1 Rotor wake geometry in ground effect

11

4.2 Interaction between the rotor wake and  
the wind in ground effect

12

4.2.1 Surface flow visualization

12

4.2.2 Smoke and flow visualization

13

4.2.3 Ground vortex strength

measurement

14

	Page
5. <u>Results and Discussion</u>	16
5.1 Rotor wake geometry investigation	16
5.1.1 General wake features	16
5.1.2 Effect of height above the ground with no wind	16
5.1.3 Effect of a forward wind velocity	17
5.1.4 Effect of number of blades with no wind	17
5.1.5 Effect of pitch angle settings	18
5.1.6 Effect of blade azimuth angle	18
5.2 Interaction between the rotor wake and the wind in ground effect	19
5.2.1 Surface flow visualization	19
5.2.1.1 General features	19
5.2.1.2 Effect of pitch angle settings and the number of blades	19
5.2.1.3 Effect of forward wind velocity	19
5.2.1.4 Effect of height above the ground	20
5.2.2 Smoke visualization and tuft grid configuration	20
5.2.3 Measurement of ground vortex strength	23
6. Proposed Future Work	24
7. Conclusions	25
8. References	26
9. Bibliography	28
10. Acknowledgements	29

## List of Figures

1. Rotor wake structure
2. Rotor wake in ground effect
3. The test-rig: photograph
4. The test-rig: layout
5. Measuring devices and ancillaries
6. Model rotor and blade profile
7. Section lift characteristic
8. Smoke visualization of two bladed rotor wake with no wind
9. Smoke visualization of two bladed rotor wake in a wind
10. Smoke visualization of five-bladed rotor wake with no wind
11. Smoke visualization of two bladed rotor wake in a wind at 90 and 270 degrees azimuth
12. Vertical velocity through the disc of two bladed rotor
13. Vertical velocity through the disc of five bladed rotor
14. Surface flow visualization of two-bladed rotor with  $\theta = 5^\circ$
15. Surface flow visualization of two-bladed rotor with  $\theta = 10^\circ$
16. Surface flow visualization of five bladed rotor with  $\theta = 10^\circ$
- 17a. Near ground tuft grid configuration
  - b. Surface flow visualization
- 18a. Front wake ground vortex smoke visualization
  - b. Downstream wake ground vortex tuft configuration
19. Measurement of tangential velocity of the ground vortex

## Introduction

Helicopter pilots find that the power required to operate close to the ground is less than that required out of the ground effect. This ground effect arises from changes in the flow underneath the rotor. When a helicopter finally lands vortices roll up on the ground, capable of causing flow disturbances powerful enough to lift debris.

We have studied the wake of the rotor and these vortices, both in still air and in a wind. In the tests, a rotor was placed above a flat ground plate with an elliptic leading edge in the working section of a 2 m diameter open tunnel.

The working section is 2.7 m long and the maximum tunnel speed was 7.6 m/s at the working section, giving an advance ratio of the rotor at 0.24.

Two rotor configurations were tested, one with two blades and a solidity ratio of 0.25, the other with five blades and a solidity ratio of 0.44.

## 1. Background

### 1.1 Rotor wake

A rotating rotor whose blade sections are at incidence will generate lift. Associated with the lift is bound circulation.

On the three dimensional blade the bound circulation is trailed into the wake from the blade tip, root and trailing edge. The shed vorticity left in the rotor wake is time variable due to the radial and azimuthal changes in lift.

Because of the increase in velocity towards the blade tip, the lift and circulation are greatest there. Since this circulation drops to zero at the tip over a short distance, its rate of decrease is very high near the tip. The result is a large trailing vorticity strength at the outer edge of the wake, causing the vortex sheet to roll up quickly into a concentrated tip vortex. The blade tip geometry also influences the formation of this tip vortex. For a square tip, most of the roll up has occurred by the time the vortex leaves the trailing edge (Ref. 2). On the inboard portion of the blade, the bound circulation drops off gradually to zero at the root. Hence in the wake, there is an inboard sheet of trailed vorticity with opposite sign to the tip vortex. Since the gradient of this bound circulation is low, the root vortex is much weaker and more diffuse than the one from the tip. The self induced velocity of the wake produces substantial distortion of the vortex filaments as they are convected with the local flow (Ref. 1). In zero forward motion (hover) the tip vortex and the remaining portion of the vortex sheet travel downwards in a smoothly contracting helical pattern determined by an induced velocity field, generated by both the wake and the blade bound vorticity, with the vortex sheet travelling downstream at a faster rate than the tip vortex. In the region of maximum wake contraction the strong interaction between adjacent tip vortices from the neighbouring rotor alters the trajectory of the vortices, causing them to move downwards at an irregular rate. Thereafter vortex instability occurs,

which eventually results in vortex diffusion and break up (Ref. 1), Fig. 1.

In horizontal forward motion, the vorticity trailed from the blade is carried rearwards and downwards. The wake geometry consists of skewed interlocking helical sheets of vorticity.

The relative positions of the rotor blade and the individual wake vortices vary periodically as the blade rotates, producing a strong variation in the wake induced velocity encountered by the blade and hence in the blade loading.

### 1.2 Ground effect on a rotor

Since a rotor derives its lift from the downward vertical momentum it imparts to the air flowing through the disc, when the downwash strikes the ground a considerable effect on the distribution of the induced velocity along the rotor blade will be experienced. On the ground the vertical velocity of the downwash flow is reduced to zero, since there can be no flow through the ground. The flow pattern of a rotor near the ground can in principle be deduced from the interaction of the slipstreams from two identical rotors producing equal but opposite thrusts. The dividing streamline of the combined flow-fields is the equivalent of the ground beneath the single rotor. This second rotor is said to be an image of the first. The vorticity components of the image rotor will induce vertical velocity components at the first rotor which will effectively reduce the induced velocity through it. Consequently the power required to produce a given thrust will be reduced.

### 1.3 Ground effect on a rotor wake

From the previous explanation, we have that at the ground, in hover, the elements of this vortex system of the wake after being reflected by the ground will for the most part continue moving radially outward along the ground.

When the rotor is operating near the ground in a wind there is a substantial change in the wake behaviour. In front of the rotor, the wake will be impeded at a certain distance by the wind, while at the rear the flow will be accelerated rearwards and the rear boundary of the wake will turn rearwards slightly above the ground. Hence the forward going portion of the wake will be stopped by the oncoming wind and roll up into a ground vortex. The wind will be deflected up and round the ground vortex.

The general nature of the flow on the ground is such as to transport this rolled up vorticity sideways and rearwards along more or less parabolic path (Ref. 5), Fig. 2.

## 2. Experimental Facilities

### 2.1 Rotor test rig

The test rig is shown in Figs. 3 and 4. This rig consists of a rotor test stand with a ground board mounted on it, and a model rotor.

#### 2.1.1 Rotor test stand

The test stand has a shaft to which a model rotor is attached driven by a single-phase electric motor through a belt drive and pulleys. The speed of the shaft is adjusted by choosing the appropriate ratio between the diameter of the two pulleys. We used in this experiment 1450 rpm which corresponds to a tip speed ( $\Omega R$ ) of 107 fps or 32.6 m/s. The shaft can be tilted manually within a range of 0 to 12 degrees. The electric current consumed by the motor is monitored by an ammeter.

Since the motor has only 1 HP power, the maximum number of blades which can be attached to the shaft is five if the complete pitch angle range of the blades, -20 to + 20 degrees, is to be available. A ground board is mounted on the frame and the shaft passes through it. The maximum possible height of the rotor above the board is 0.8 rotor diameters.

2.1.2 Model rotor

	Rotor 1	Rotor 2
Diameter (m)	0.43	0.43
Number of blades	2	5
Solidity ratio	0.25	0.44
Hub diameter	0.15	0.15
Blade root diameter (m)	0.15	0.15
Tip speed (m/s)	32.6	32.6
Blade profile	- High cambered aerofoil 10% thick -	
Blade chord (m)	0.065	0.065
Tip form	square	square

Section co-ordinates		
X/C	Y/C upper	Y/C lower
0	0.03	0
0.077	0.092	0.023
0.154	0.123	0.031
0.230	0.138	0.046
0.308	0.150	0.050
0.385	0.157	0.054
0.462	0.154	0.052
0.538	0.150	0.046
0.615	0.138	0.045
0.692	0.123	0.040
0.769	0.108	0.031
0.846	0.085	0.023
0.923	0.062	0.015
1.000	0.015	0

(See Fig. 6)

The section's lift characteristic is shown in Fig. 7.

## 2.2 Measuring devices and ancillaries

These are shown in Fig. 5.

Measuring devices (pressures and velocities):

- standard pitot and static tubes
- five-hole pressure probe
- fine pitot and static tube
- Betz manometer and micromanometer

Ancillaries are:

- smoke generator and its nozzle
- tuft grid mounted on a solid frame
- pitch angle protractor
- manual traversing mechanism for the probes

## 2.3 Photographic equipment

A high speed polaroid camera with flash is used to make instant photographs of the flow. The advantage of the instant camera is that we can immediately be sure whether or not a photograph can record the flow behaviour clearly. If it can, more photographs are taken using an ordinary single lens reflex camera with flash.

## 2.4 Windtunnel

An open working section tunnel was allocated for these experiments. It has a diameter of 2 m, a working space length of 2.7 m and a return collector of 1.6 m. Tunnel speed is adjusted smoothly by means of a resistor control device, and the maximum speed obtainable in the working section is 7.6 m/s.

### 3. Experimental Technique

#### 3.1 Flow visualization

To visualize the flow, three methods were used.

1. Smoke visualization, to show the movement of the flow in two-dimensions.
2. Surface flow visualization, to show the movement of the flow on the ground or on a horizontal plane.
3. Tuft grid, to show the local flow direction in three-dimensional flow conditions.

##### 3.1.1 Smoke visualization

In principle this method calls for the insertion of very small particles of fluid into the object air to mark the flow features without changing the density or other properties of the air itself. For a flow in air, a convenient way is to mix smoke with the airstream. The smoke is provided by a smoke generator with a hot, electrically heated tip which evaporates vegetable oil forced to flow through the tip by the pressure in the oil tank. Care has to be taken that the smoke does not impart an increased velocity to the flow.

Tip vortex and ground vortex are especially suitable subjects to be shown by the smoke method. We also have to realize that sometimes, although the smoke can record the flow movement, it may not be seen by the naked eye. This usually happens in an unsteady flow which has a fluctuating frequency higher than our eyes can detect. This needs photographic equipment to record it, using a shutter speed higher than fluctuating frequency so that the movement can be halted and seen from the still photographic result. Rotor flow is an example of such an unsteady flow due to its solidity ratio being much less than one. Photographic records of the flow will disclose many facts which cannot be obtained by visual observation.

### 3.1.2 Surface flow visualization

A special quick dry paint made from titanium dioxide powder mixed with raw linseed oil and then lightened by adding paraffin, is painted on the surface. When there is an air flow moving on the surface, the paraffin will evaporate, leaving the paste to mark the streaklines. This method shows very clearly the region on the ground where the oncoming wind meets the rotor wake. The direction of the flow in any particular area of the surface can be traced from the streaklines.

### 3.1.3 Tuft grid visualization

This is the simplest way to obtain a rough picture of the flow using very thin and light threads of silk which are quite floppy. In a three-dimensional flow the smoke can easily be diffused and a tuft grid is more applicable. Although it is a simple device, the three components of a three-dimensional flow can be shown simultaneously by the tufts attached to a network of fine wires which are held in a solid frame.

### 3.2 Velocity measurement technique

In the experiment three particular air velocities were measured.

- The tunnel speed to find the value of the advance ratio  $\mu$ .
- The tangential component of velocity  $q_t$ , tangential to the core of the ground vortex, which would be used to estimate its strength.
- The vertical component of induced velocity through the disc.

This means that we had to deal with two different conditions of the flow; firstly the steady tunnel flow, and secondly the unsteady ground vortex and rotor downwash flow, which were quite sensitive to probes inserted into them.

### 3.2.1 Measurement of the tunnel speed

The speed of the tunnel flow was measured directly by a standard pitot static tube connected to a Betz manometer. The local air density was corrected against local temperature and local barometric pressure, which for the open tunnel equals the static pressure. Care was taken to align the pitot static tube with the flow direction.

### 3.2.2 Measurement of the vortex tangential velocity

A standard pitot static tube is too big to measure the velocity tangential to the vortex core because of the disturbance it would cause. Instead two fine pitot and static tubes were used to measure static and stagnation pressure separately. These tubes were always positioned tangential to the vortex core and neglected the axial component of the vortex. To position the tubes we used a pitch angle protractor.

### 3.2.3 Measurement of vertical velocity through the disc

This vertical velocity is the vertical component of the inflow velocity. Although the flow was also unsteady due to the low solidity of the rotor, it was not usually as easily disturbed as the tangential velocity of the ground vortex. Exceptions could occur near the tip where tip vortex might strike the measuring tubes. We used the fine pressure tubes again to measure the dynamic pressure and hence the velocity. Care was taken to ensure that the fine probe was exactly perpendicular to the rotor disc plane and as close as possible to the rotor. The probe was positioned using the protractor.

#### 4. Experimental Programme

The fixed bladed rotor was tested close to a fixed ground board in the open working section of a low speed wind tunnel at speeds up to 7.6 m/s. Particular attention was paid to the interaction of the rotor slipstream with the oncoming wind, the impact of the slipstream on the ground, and the development of the ground vortex.

##### 4.1 Rotor wake geometry in ground effect

The aim was to see how the rotor created its wake, and what shape it took in the proximity of the ground. The wake of the rotor is very complex. It consists of the vortex sheet left by each individual blade, which then move downstream away from the rotor disc, at the same time distorting quite considerably under their own influence. Since the solidity of the rotor is much less than one, the wake is time dependent and the downwash flow is not steady. Smoke visualization was used to show the shape of the wake, and vertical velocity through the disc was measured.

##### Test procedure:

1. Run the model rotor at 1450 rpm.  
The test rig had to be isolated from excessive vibration, since this would create more substantial disturbances.
2. With the rotor in continuous and steady rotation, smoke was injected into the flow just above the rotor tip. The smoke captured by the vortex cores, visually identifies the tip vortex pattern at different azimuth positions relative to the blade. The wake boundaries were identified by the vortex filaments from the rotor tips.
3. The vortex pattern was then photographed from one position. The camera had to be perpendicular to the plane which was formed by the shaft and the azimuth rotor position where the smoke was fed in.

4. Vertical velocities through the disc were then measured at points along the span to show its variation from the root to the tip of the rotor. Measurements were taken in the region very close under the disc to avoid direct contact with the spiralling tip vortices in the near wake.
5. This was repeated for various heights above the ground, various pitch angle settings and two model rotors of different solidity.
6. The procedure was repeated with the wind on to show the effect of an oncoming wind on the wake shape.

#### 4.2 Interaction between the rotor wake and the wind in ground effect

In section 1 we emphasised that the rotor wake is dominated by the tip vortices. With no cross wind the elements of the vortex system in the slipstream will for the most part move outward radially along the ground.

In a cross wind the forward development of the wake of the rotor will be opposed by the wind. The forward slipstream will roll up on the ground then stream back with the wind around the rear slipstream.

Three methods were used to investigate this flow.

##### 4.2.1 Surface flow visualization

The aim was to show the details of the flow on the ground and to locate where the slipstream would roll up and stream back on the ground behind the rotor.

Ref. 7 has identified that there is an interaction boundary between the two opposing flows. The inner curve of the interaction boundary marks the front boundary of the ground vortices. Surface flow visualization locates the position of this interaction boundary on the ground.

### Test procedure

1. Paint the ground board with titanium dioxide paint in a thin even layer.
2. Run the tunnel until a steady velocity has been obtained.
3. Run the rotor to speed.
4. After the large part of the paraffin on the paint has evaporated and the paint is rather dry, the rotor and the tunnel are stopped at the same time.
5. Flow pattern on the ground is then measured and analysed.

These tests were carried out with the rotor at different heights above the ground, with rotors with 2 and 5 blades, and over a range of tunnel speed.

#### 4.2.2 Smoke and tuft grid visualization

The surface flow visualization identified the boundary at the ground vortex but did not locate its core.

Smoke emitted into the flow at the forward position of the ground vortex visualized the vortices on the boundary of the rotor slipstream and the rolled up ground vortex (Fig. 19a). The smoke was unable to follow the path of the ground vortex as it streamed back from the rotor because it diffused rapidly. A tuft grid was used to locate the core of the ground vortex as it streamed back.

#### Test procedure:

- a. A surface flow visualization of the interaction boundary had been obtained for a particular condition of tunnel and rotor speed. The inner line of this boundary was the leading edges of the ground vortices (Ref. 7). The tunnel and the rotor were run again at the same speed as had produced the surface visualization result.
- b. Smoke is emitted into the flow from a smoke generator placed ahead of the shaft, above the interaction boundary.

- c. We can see the ground vortices developing from the smoke configuration. The smoke nozzle is then positioned tangential to the ground vortex core and parallel to the ground. The smoke defines the core size.
- d. Downstream of the rotor, a tuft grid placed perpendicular to the interaction boundary locates the vortex core. The tuft grid is large enough to contain the vortex core so that an estimate of its diameter can be made.

#### 4.2.3 Ground vortex strength measurement

Knowing the core diameter of the ground vortex, its strength was estimated as in Ref. 2 by applying the following relation:

$$K = 2\pi r q_t$$

where  $K$  = vortex strength

$r$  = vortex core radius

$q_t$  = velocity at  $r$  tangential to the core

Note that in Ref. 2, the core diameter was defined by the positions of the maximum tangential velocity.

In the present experiment the tangential velocity was measured only on the boundary of the vortex core. Fine pitot and static tubes were used to measure total and static pressure at the same position, with as little interference to the flow as possible (Fig. 19b).

From the smoke visualization it was observed that the ground vortex floats above the ground. It experiences a downward vertical self-induced velocity and a boundary-induced upwash velocity (Ref. 5).

To avoid these two velocities confusing the issue, measurements were taken at the upper and bottom points of the core, and not at side points (Fig. 19).

$$q_t = \sqrt{2(P_{\text{total}} - P_{\text{static}})/\rho}$$

$\rho$  is the local air density corrected to the local pressure and temperature.

The effect of changes in the tunnel velocity and rotor height above the ground, on the ground vortex strength were investigated.

The free stream velocity was measured with the rotor at rest just ahead of the known position of the rotor wake. No tunnel speed correction was needed.

## 5. Results and Discussion

### 5.1 Rotor wake geometry investigation

#### 5.1.1 General wake features

Smoke visualization pictures in the no-wind condition (Figs. 8a and 8b) show a common wake shape. Initially in ground effect the rotor wake contracts rapidly and keeps the strong tip vortex close to the rotor disc, maximising its effect on the inflow velocity through the disc. The velocity measurement at the disc shows a strong tip vortex inboard of the blade tip. On reacting the ground the rotor wake then expands radially outward.

#### 5.1.2 Effect of height above the ground with no wind

From the smoke pictures (Figs. 8a and 8b) we can see how the strong tip vortices which dominate the wake travel further outward from the rotor at the lower height than from the higher one. We can interpret this as suggesting that the wake is stronger if the rotor is nearer to the ground. Further discussion may be found in Section 5.1.6. Vertical velocity measurements show that at  $Z/D = 0.3$  the vertical velocity through the disc was less than at  $Z/D = 0.5$ . As the ground effect reduced the velocity, the ammeter measurements showed that it also reduced the power requirement.

Blade element theory gives the blade sectional incidence as

$$\alpha(r) = \theta - \phi(r) = \theta - V_i/\Omega R$$

where  $\alpha$  = local blade incidence  
 $\theta$  = blade pitch angle, constant for the untwisted blade  
 $\phi$  = inflow angle  
 $V_i$  = vertical velocity through the disc  
 $\Omega R$  = blade tip speed

With a reduction in  $V_1$  and a constant blade pitch angle, the blade incidence increases so that the blade section generates more lift for the same input power. This reduction in velocity and increase in incidence as the height is reduced from  $Z/D = 0.5$  to  $0.3$  is quite substantial. Ground proximity leads to a substantial lift augmentation. It is well known that the effect falls off rapidly with height and has disappeared around a rotor diameter above the ground (Ref. 8).

#### 5.1.3 Effect of a forward wind velocity

In Figs 9a and 9b, the smoke pictures show how the forward wind pushed the rotor wake downstream creating a wake skew angle, the angle of the wake to the rotor disc. In Fig. 9a an upwash in the region near the tip is visualized. This shows that the initial flow path ahead of the rotor was upward then downward through the disc into the rotor slipstream, causing changes in the blade induced velocity distribution. The wake from the rotor closer to the ground, Fig. 9a, was less deflected by the wind. The velocity measurements (Fig. 12) show that the wind caused the velocity to increase. At  $Z/D = 0.3$ , the wind increased the vertical velocity through the disc to a value of almost the velocity at  $Z/D = 0.5$  in the no wind condition. This implies that in the no wind condition, benefits from the ground in creating extra lift can be felt up to a greater height than in a forward wind.

#### 5.1.4 Effect of number of blades with no wind

The smoke pictures in Figs. 10a and 10b show the wake of the five bladed rotor (rotor II) at  $Z/D = 0.3$  and  $0.5$ . The wake is much more diffuse than in the two-bladed case. The spacing between the blades is much smaller so that the tip vortices are closer and interact more strongly. The rolled up vortices in the wake of the two bladed rotor are further apart (Fig. 8) than they are in that of the five bladed rotor

(Fig. 10), where they touch each other. This touching appears to diffuse the vortices so that they break up.

#### 5.1.5 Effect of pitch angle settings

Figs 12 and 13 compare the velocities measured beneath two-bladed and five-bladed rotors at pitch angles of  $5^\circ$  and  $10^\circ$ . At the higher pitch the rotor develops more thrust and imparts more vertical momentum to the rotor wake. This shows in the increased vertical velocities with the increased pitch at a given height above the ground. Note also that for a given pitch setting the inflow velocities beneath the rotor decrease closer to the ground.

#### 5.1.6 Effect of blade azimuth angle

In Ref. 1 Landgrebe shows that the far wake region of a hovering rotor is not stable since it undergoes a kind of viscous dissipation.

The smoke pictures in Figs. 8a and 8b confirm that. We see only three vortices in the wake and the third is already slightly diffused. Figs. 11a and 11b show the tip vortices when the rotor blades were at approximately  $90^\circ$  and  $270^\circ$  azimuth angle. Comparing these with Figs. 8a and 8b, we observe that the stable tip vortices when the blades are at  $0^\circ$  and  $180^\circ$  azimuth angle are further out from the shaft than in the  $90^\circ/270^\circ$  case. When the advancing blade is at  $180^\circ$  azimuth the forward wind deflects the rotor wake less than when the advancing blade is at  $90^\circ$  azimuth. Since on the ground the interaction between the wake and the wind generates a ground vortex, we might expect the ground vortex strength to vary with azimuthal changes of the rotor blades.

## 5.2 Interaction between the rotor wake and the wind in ground effect

### 5.2.1 Surface flow visualization

#### 5.2.1.1 General features

A surface flow visualization, Fig. 17b, clearly identifies the limit of the outward flow of the rotor wake against the forward velocity of the tunnel. Behind this interaction boundary the surface streaklines show the flow moves radially outward.

This interaction boundary has approximately a parabolic shape as in Ref. 5. Fig 17a shows a ground board tuft grid. The flow out from the rotor stops and in the interaction boundary region the tufts go limp. At the boundary the tunnel flow is deflected and continues downstream.

#### 5.2.1.2 Effect of pitch angle settings and the number of blades

Compare Fig. 14, a surface flow visualization of a two-bladed rotor as a  $5^{\circ}$  pitch angle, with Fig. 15, one of a two bladed rotor at a  $10^{\circ}$  pitch angle. The interaction boundary of the rotor with the higher pitch angle is always further outward for a given tunnel speed. The more loaded rotor has a further forward position of the boundary

#### 5.2.1.3 Effect of forward wind velocity

Figs. 14, 15 and 16 show that the higher the forward wind velocity the more the wake is deflected and the less far forward is its interaction boundary. The stronger this wind the more and more asymmetrical becomes the shape of the interaction boundary. The advancing side is always further outward than the retreating side. This is due to the fact that with fixed blades the advancing side produced more lift than the retreating side so that the wake on the advancing side has higher inflow velocities.

#### 5.2.1.4 Effect of height above the ground

The higher the rotor is from the ground, the less the wake can resist the forward wind, the nearer the interaction boundary comes to the shaft and the more asymmetric is the boundary. Recalling the discussion in 5.1.6 we note that the further the vortex system is from the rotor the weaker it becomes and the more easily it diffuses.

#### 5.2.2 Smoke visualisation and tuft grid configuration

Fig. 18a shows a ground vortex near the interaction boundary in the forward wake region, rolling up clear of the ground. Heyson (Ref. 5) found that the self induced vertical velocity at the wake in ground effect is in equilibrium with the boundary induced upwash, so that the ground vortex floats above the ground with no further downward movement.

In Fig. 18b the tuft grid shows a section through the ground vortex at three rotor radii distance behind the rotor shaft. Such sections yield the diameters of the ground vortex cores and the height above the ground of the centre of these vortex cores. For simplicity the ground vortex can be taken to have a circular cross section. Velocity measurements were taken through the core of the vortex and the central core identified by the fall to zero of this velocity (Table 5.1).

From these measurements we were able to position the pitot and static probes to find the tangential velocities of the ground vortices in the downstream region. At three rotor radii distance downstream, the diameter of the ground vortex was the same as in the forward wake, but the centre of the core was slightly higher from the ground. It is likely that this happened due to the thickening of the boundary layer on the ground board in the downstream region.

Table 5.1

Forward wake measurement station.

Rotor	$\mu$	h (m)	r (m)	$q_t$ (m/s)	K (m <sup>2</sup> /s)
2 blade	0.1	0.045	0.0275	4.04	0.7
Z/D = 0.3	0.15	0.045	0.03	5.8	1.09
$\theta = 10^\circ$	0.2	0.050	0.025	3.7	0.58
2 blade	0.1	0.042	0.025	2.35	0.37
Z/D = 0.5	0.15	0.042	0.025	2.15	0.34
$\theta = 10^\circ$					
5 blade	0.1	0.045	0.02	1.35	0.17
Z/D = 0.3	0.15	0.045	0.022	2.19	0.3
$\theta = 10^\circ$	0.2	0.0475	0.022	2.86	0.4
5 blade	0.1	0.045	0.02	1.35	0.17
Z/D = 0.5	0.15	0.045	0.02	1.18	0.15
$\theta = 10^\circ$					

Downstream wake measurement station.

(3 rotor radii behind the shaft)

2 blade	0.1	0.05	0.025	4.04	0.63
Z/D = 0.3	0.15	0.05	0.03	4.38	0.83
$\theta = 10^\circ$	0.2	0.05	0.03	4.7	0.89
2 blade	0.1	0.052	0.025	3.7	0.58
Z/D = 0.5	0.15	0.055	0.025	4.04	0.63
$\theta = 10^\circ$	0.2	0.055	0.025	4.38	0.69

Notation:

$q_t$  = ground vortex tangential velocity

$\mu$  = advance ratio

h = distance from the centre of ground vortex  
to the ground

r = radius of ground vortex

K = ground vortex strength

### 5.2.3 Measurement of ground vortex strength

Table 5.1 tabulates the measurements of the ground vortex tangential velocities and the estimates of its strength. The tangential velocities  $q_t$  were measured at the top and bottom of the vortex cores. To estimate the vortex strength an average of these two measurements was used as the tangential velocity  $q_t$  representing the vortex core. The vortex strength  $K$  was approximated by  $2\pi q_t$  times the radius of the core. At the forward wake measuring station, the ground vortex strength appears to reach a maximum as the advance ratio ( $\mu$ ) increases before decreasing with further increase of  $\mu$ .

The vortex cores are a constant height above the ground over the range of advance ratio tested.

Fig. 15 shows the interaction boundary at  $\mu = 0.2$  is no longer symmetrical as at  $\mu = 0.15$  and that it comes nearer to the shaft in its distorted form. This suggests that at  $\mu = 0.2$  the front portion of the wake was about to turn fully rearward and at a slight higher  $\mu$  would no longer hit the ground to lose its strength. At the downstream wake measuring station the ground vortex strength increases with increasing advance ratio and the vortex cores remain at a constant height above the ground, slightly higher than at the forward station.

Many simplifications have been required to make it possible to interpret the results. The vortex tangential velocity has always been measured at the top and bottom edge of the core to avoid complication due to the presence of the self induced velocity of the vortex and the boundary induced upwash from the ground. At the chosen measuring points these two induced components do not affect the tangential velocity.

The vortex cores were taken to be clear of the ground boundary layer so that it did not influence the measured tangential velocities. The reading from the micromanometer were always recorded at their maximum value. In doing so, we ignored the time

variations in the wake due to the aximuthal changes of the vortex system shed by the blades this maximum reading was attained when the vortex was clearly shown by the smoke visualization.

Care was taken to locate the ground vortices by flow visualization, using smoke and tufts and by surface flow visualization. The ground vortex measurement section was taken perpendicular to the interaction boundary but for simplicity in estimating its strength the shape of the vortex was assumed to be circular, as in Ref. 7, and an average tangential velocity measured for that circular section. Any disturbance caused by the presence of the probe was not allowed for. The estimate of this maximum strength of the ground vortex is clearly a rough approximation.

6. Proposed future work

The work so far has only given a very approximate picture of the flow field. It is proposed to extend the measurements using an articulated rotor and hot wire velocity probes in a larger wind tunnel.

It is hoped to reduce the asymmetries observed in these experiments by using a rotor with a flapping freedom to even out the load in the advancing and retreating sectors of the rotor disc.

Thrust on the rotor will be measured directly by strain gauge balances.

A three element (triple-sensor) hot wire probe will provide a clearer and more detailed study of the flow field. Traverses will be made by a computer controlled traverse gear. The time history of this velocity field will be recorded by a high speed data acquisition system.

The larger windtunnel should allow us to observe a longer length of the ground vortex development.

The boundary layer on the fixed ground board and its effect on the flowfield will be checked.

## 7. Conclusions

A ground vortex is formed by the interaction of a rotor wake and the wind in the proximity of the ground, and its geometry is strongly influenced by a forward wind. If the forward wind velocity is sufficiently low the rotor wake is able to travel forward into the wind before rolling up into the vortex and being swept downstream. For a given rotor power the interaction boundary is swept progressively downstream under the rotor disc as the forward wind velocity increases.

The ground vortex core floats just above the ground. Its strength appears to reach a maximum with increasing forward wind velocity before decreasing with further increase in wind velocity. For the fixed rotor used the interaction boundary is asymmetric as a result of the different loads on the advancing and retreating sides of the rotor disc. Excessive noise and vibration were noted as this asymmetry increased.

Measurements have shown that the beneficial effects of the ground on the velocity through the rotor disc decreased rapidly with an increase of rotor height and forward wind velocity.

8. References

1. LANDGREBE, A.J.                   The wake geometry of a hovering helicopter rotor and its influence on rotor performance.  
Journal of American Helicopter Society. Vol. 17 No. 4, October 1972
  
2. TANGLER, J.L.  
WOHLFELD, R.M.  
MILEY, S.J.                         An experimental investigation of vortex stability, tip shapes, compressibility and noise for hovering model rotors.  
NASA CR-2305, September 1973
  
3. SIMONS, I.A.                     Blade vortex interactions on helicopter rotors in forward flight.  
Southampton University Memorandum ISAV 126, July 1965
  
4. HEYSON, H.H.                    Ground effect for lifting rotors in forward flight.  
NASA TN D-234, December 1959
  
5. HEYSON, H.H.                    Theoretical study of conditions limiting V/STOL testing in wind tunnels with a solid floor.  
NASA TN D-5819, June 1970
  
6. BRAMWELL, A.R.S.                On the static pressure in the wake of a hovering rotor.  
Vertica, Vol. 1, No. 3, 1977
  
7. WIESNER, W.                     Tail rotor performance in presence of main rotor, ground and winds.  
Journal of American Helicopter Society, Vol. 19, No. 3, July 1974

8. CHEESEMAN, I.C.  
BENNET, W.E.

The effect of the ground on a  
helicopter rotor in forward  
flight.

ARC R & M 3021, 1957

9. Bibliography

BRAMWELL, A.R.S.

Helicopter Dynamics.  
Edward Arnold, 1976

FRADENBURGH, E.A.

The Helicopter as a Ground Effect  
Machine.  
The Princeton University Conference -  
Symposium on Ground Effect Phenomena,  
October 1959

GESSOW, A.  
MEYERS, G.C.

Aerodynamics of the helicopter.  
Frederick Ungar Publishing Co,  
fifth printing 1978

GRAY, R.B.

Experimental smoke and electro-  
magnetic analog study of induced  
flow field about a model rotor in  
steady flight within ground effects.  
NASA TN D-458, December 1960

JOHNSON, W.

Helicopter Theory.  
Princeton University Press, 1980

10. Acknowledgements

The work of E.W. Osbourn in the design and construction of the test-rig is gratefully acknowledged, as is that of W. Munn as the windtunnel assistant.

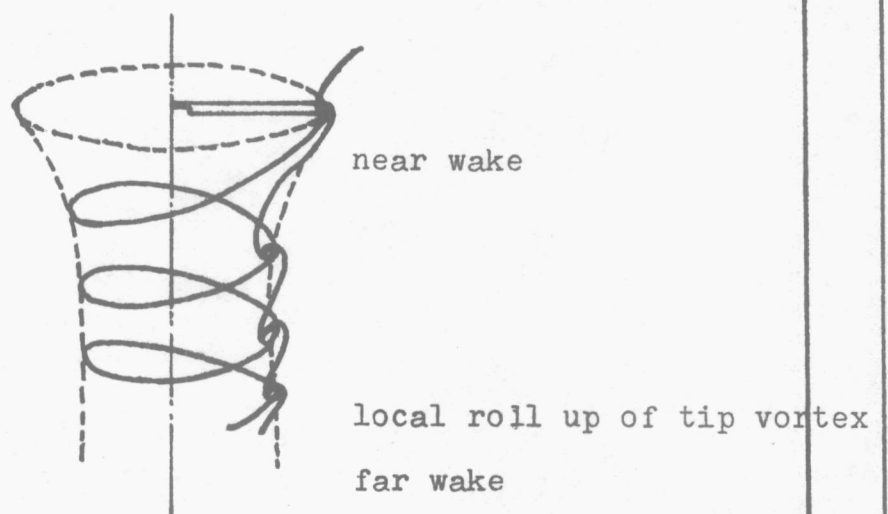
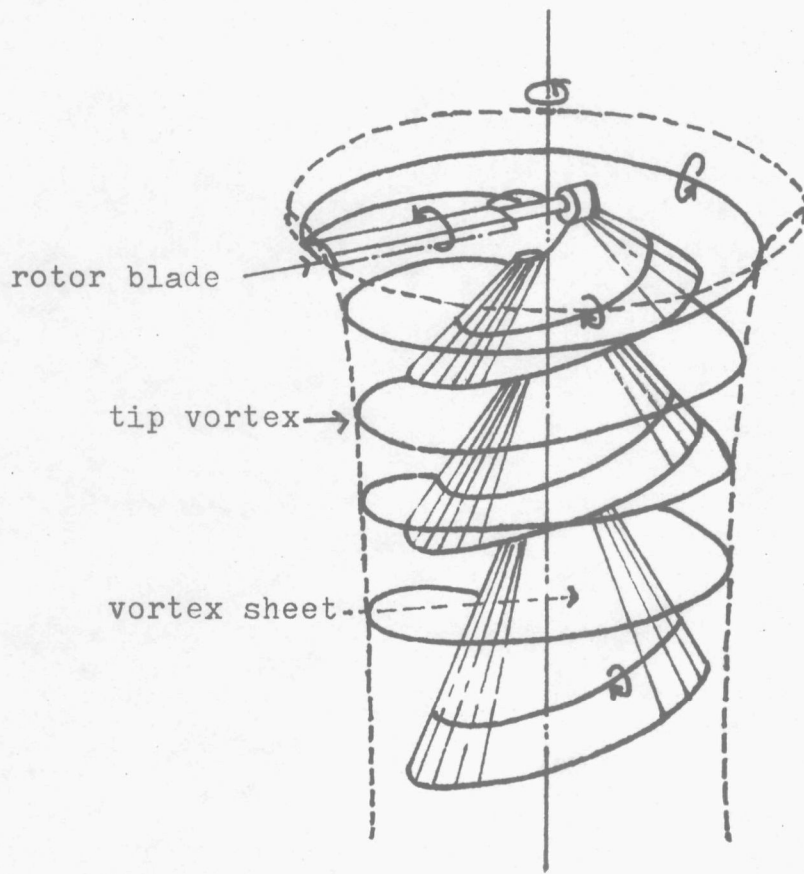


Fig 1 Rotor wake structure

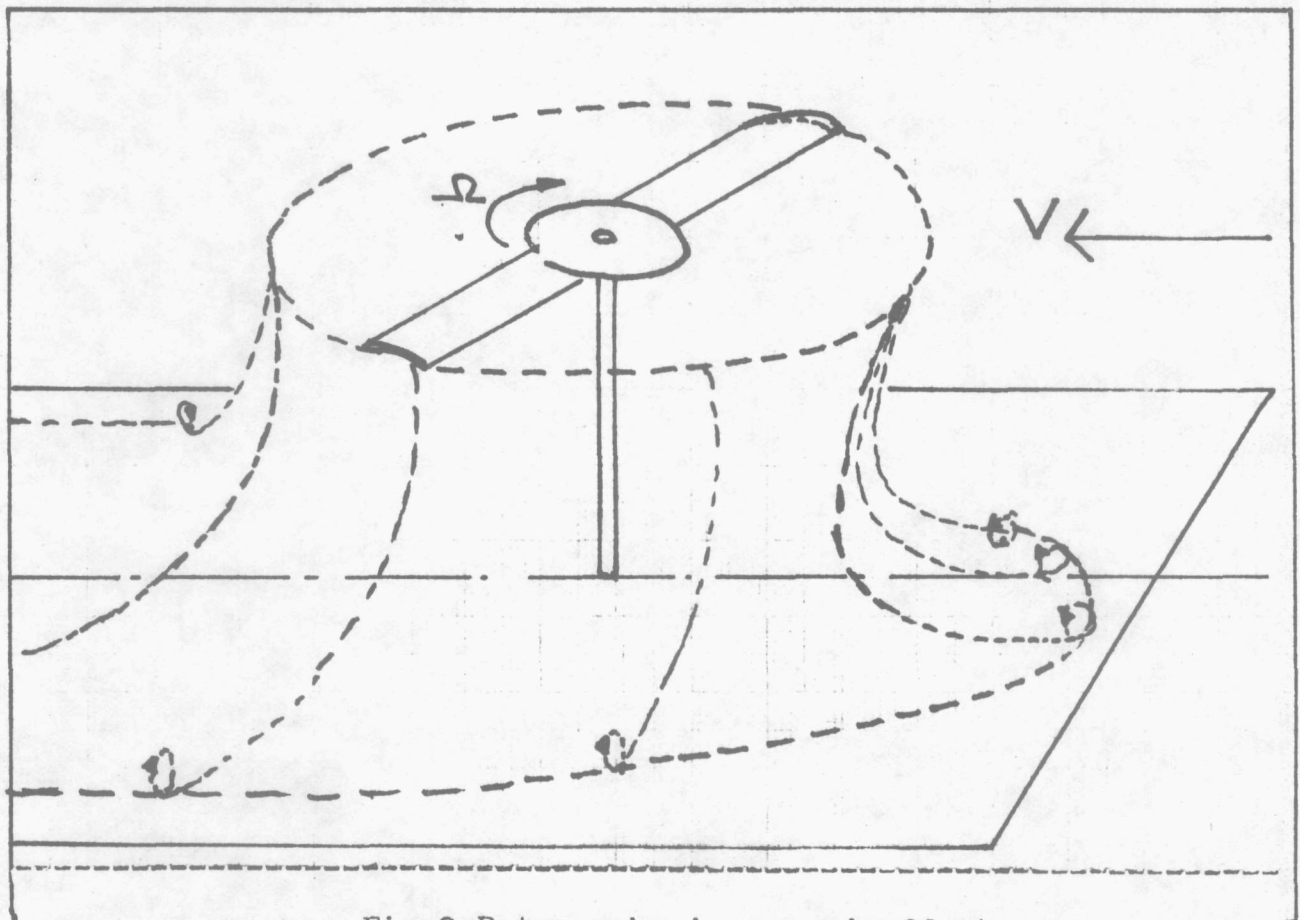
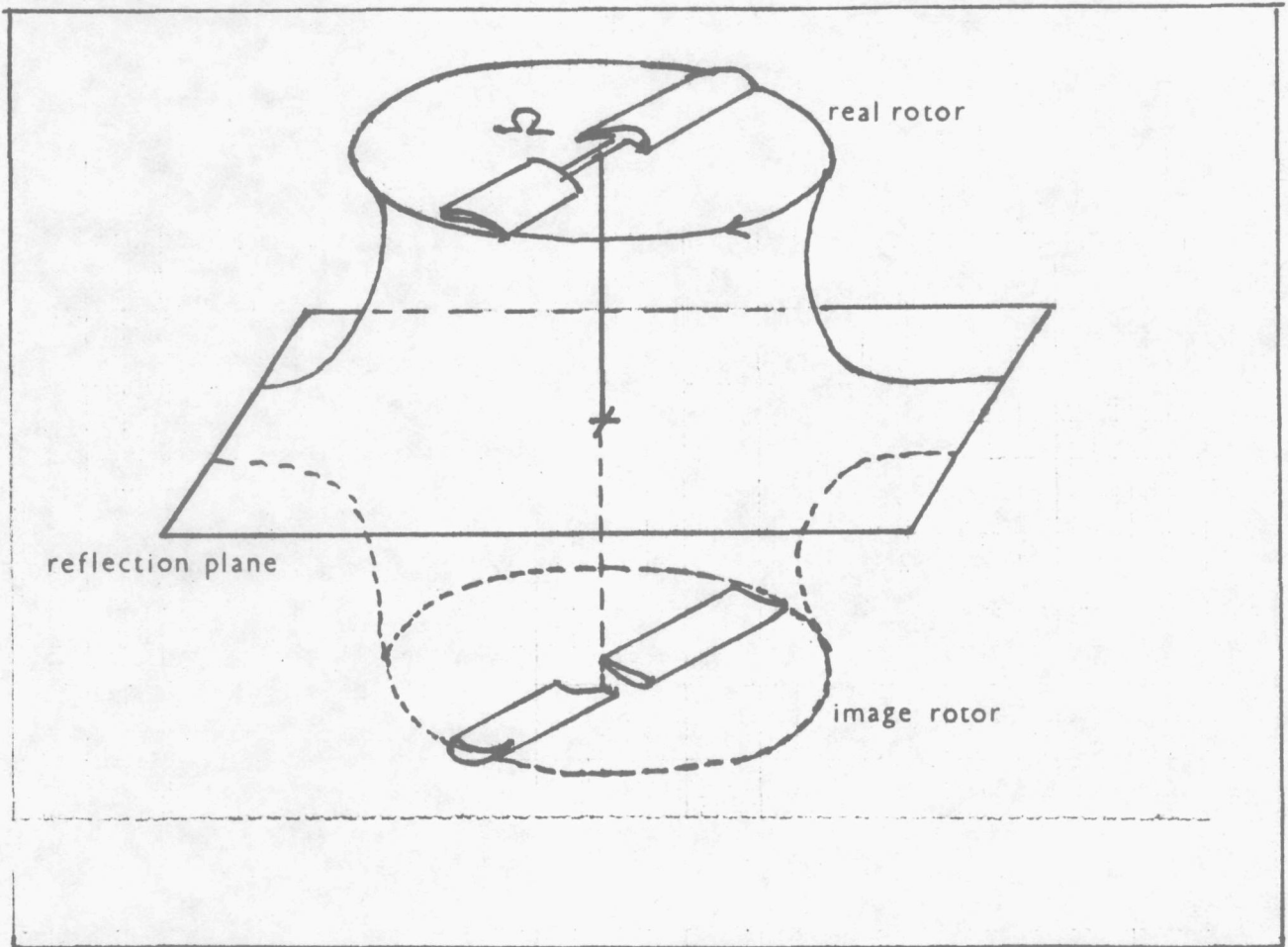


Fig 2 Rotor wake in ground effect

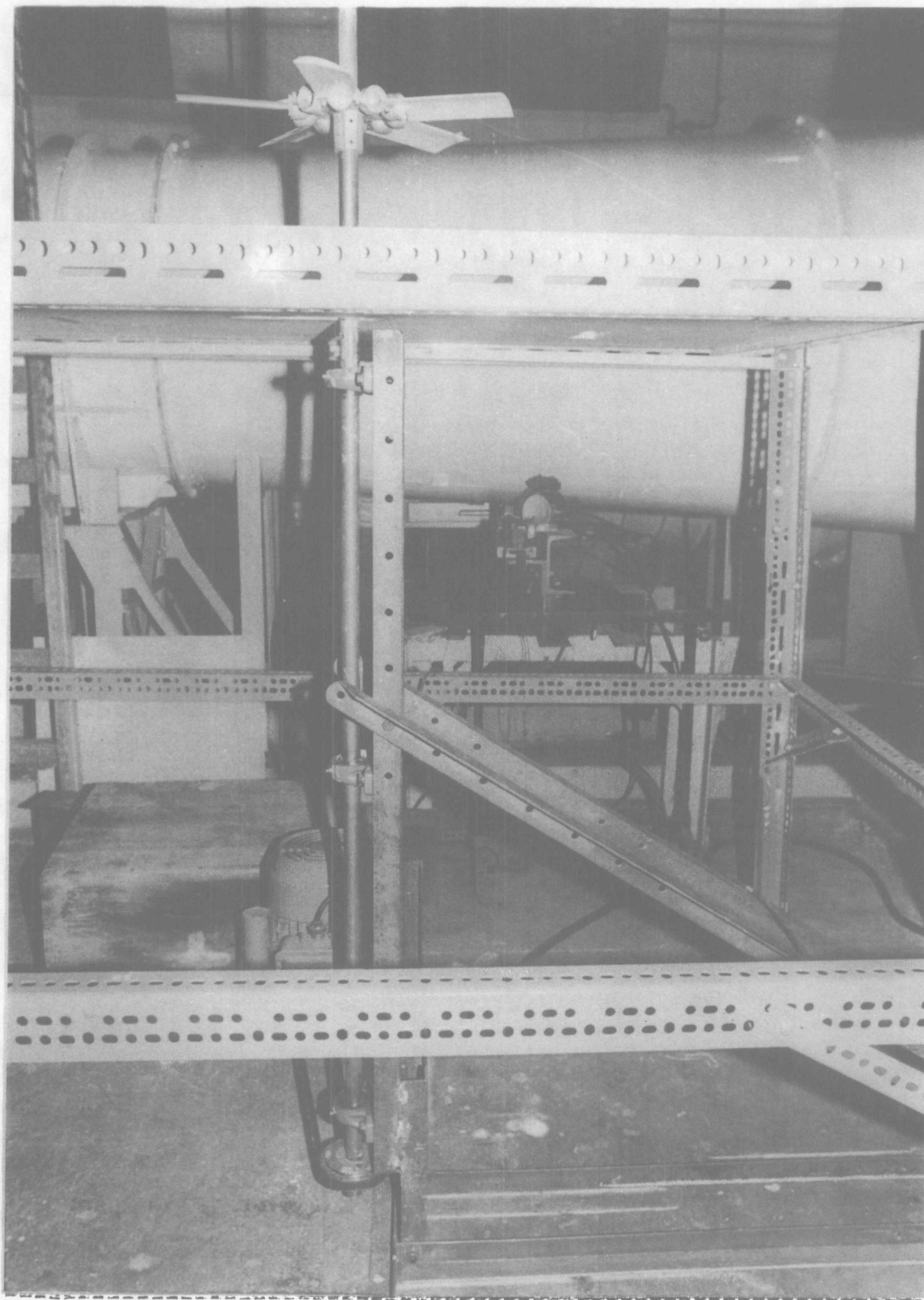


Fig 3 The test rig

---

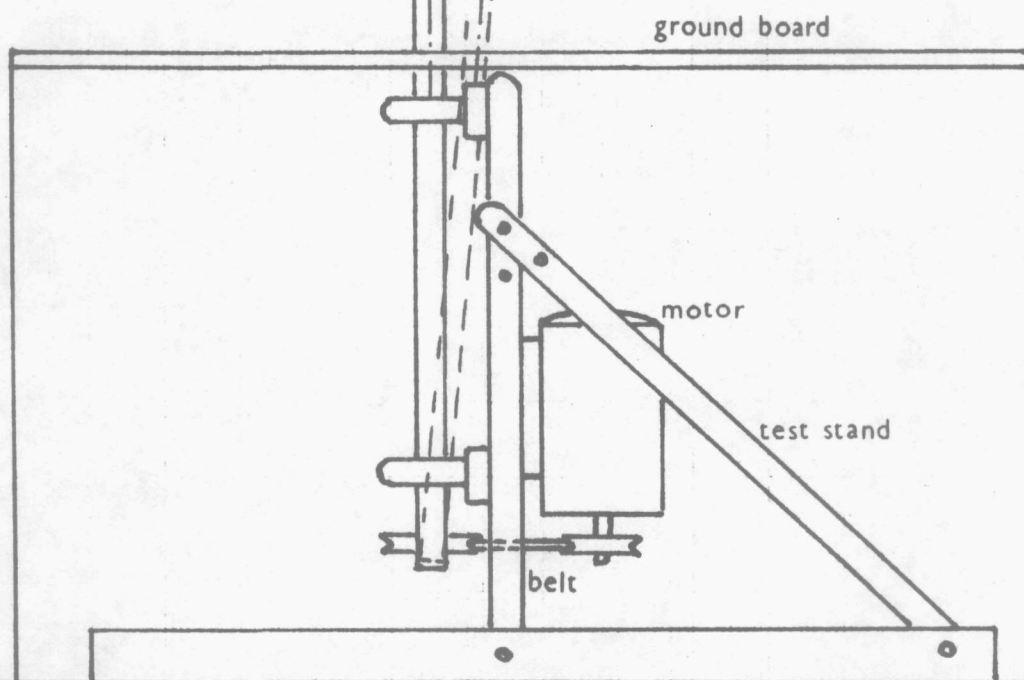
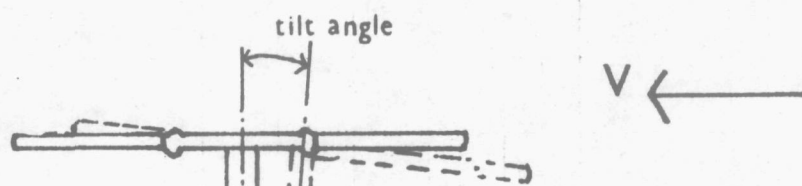
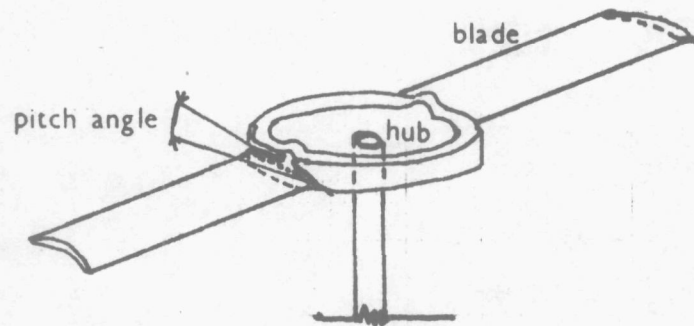


Fig 4 The test rig

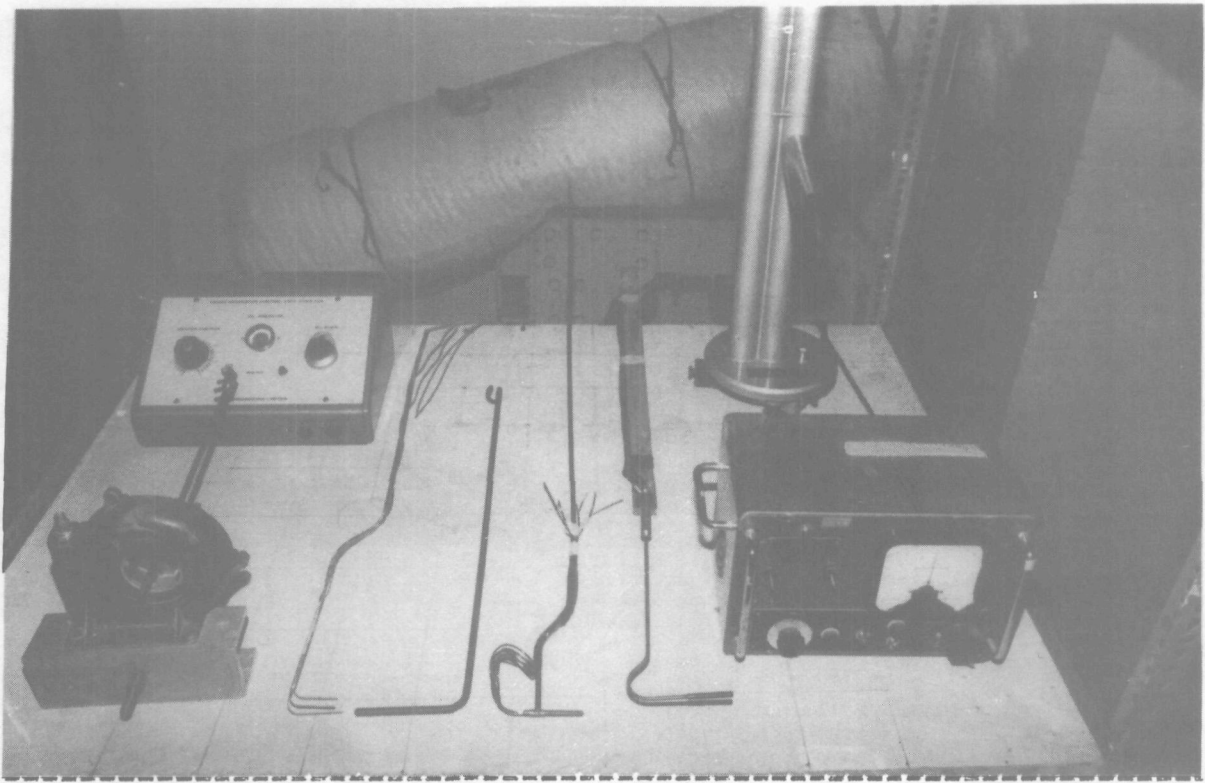


Fig 5 Measuring devices and ancillaries

---

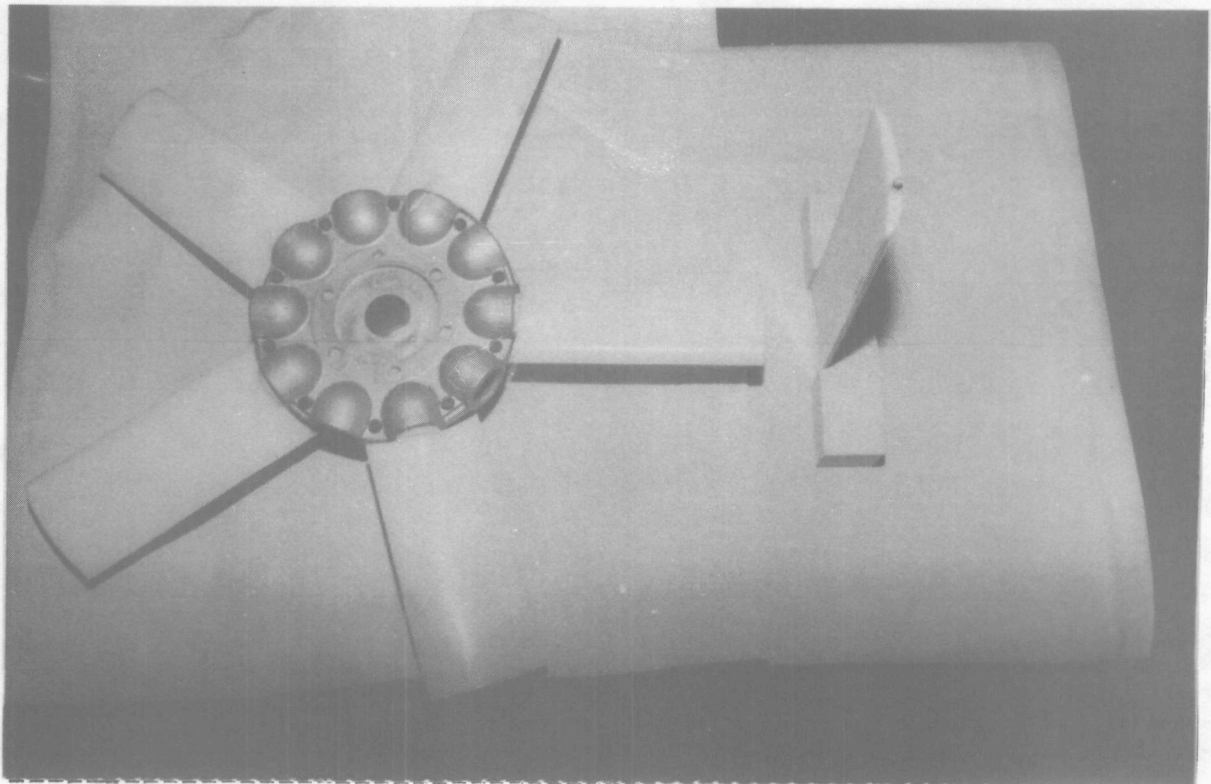
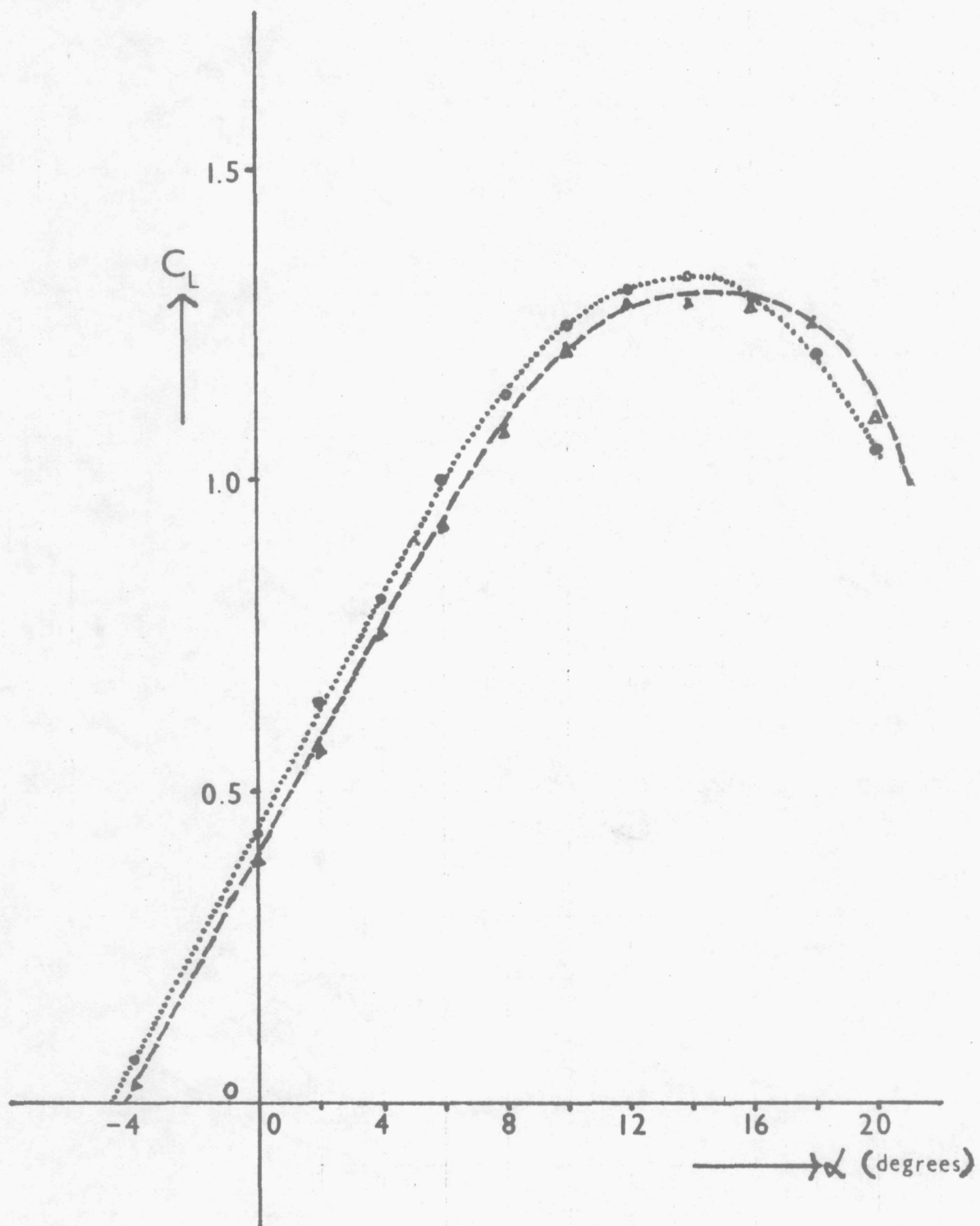


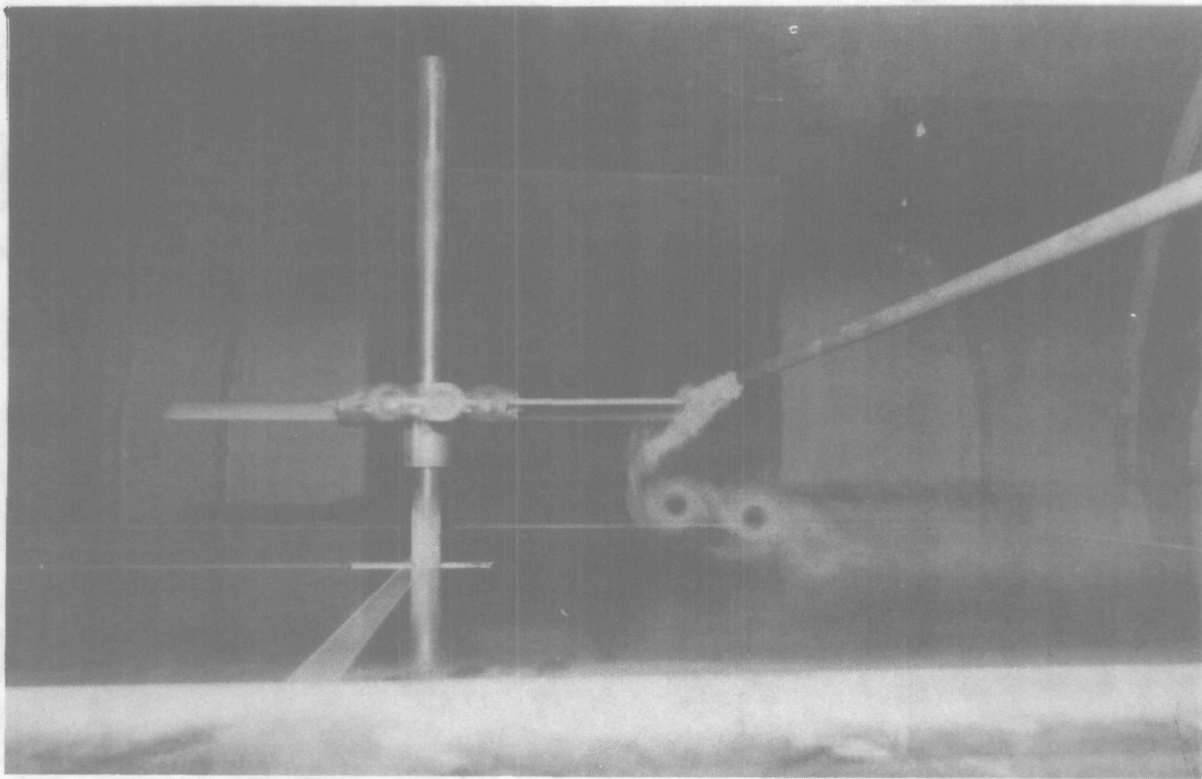
Fig 6 Model rotor and blade profile

---



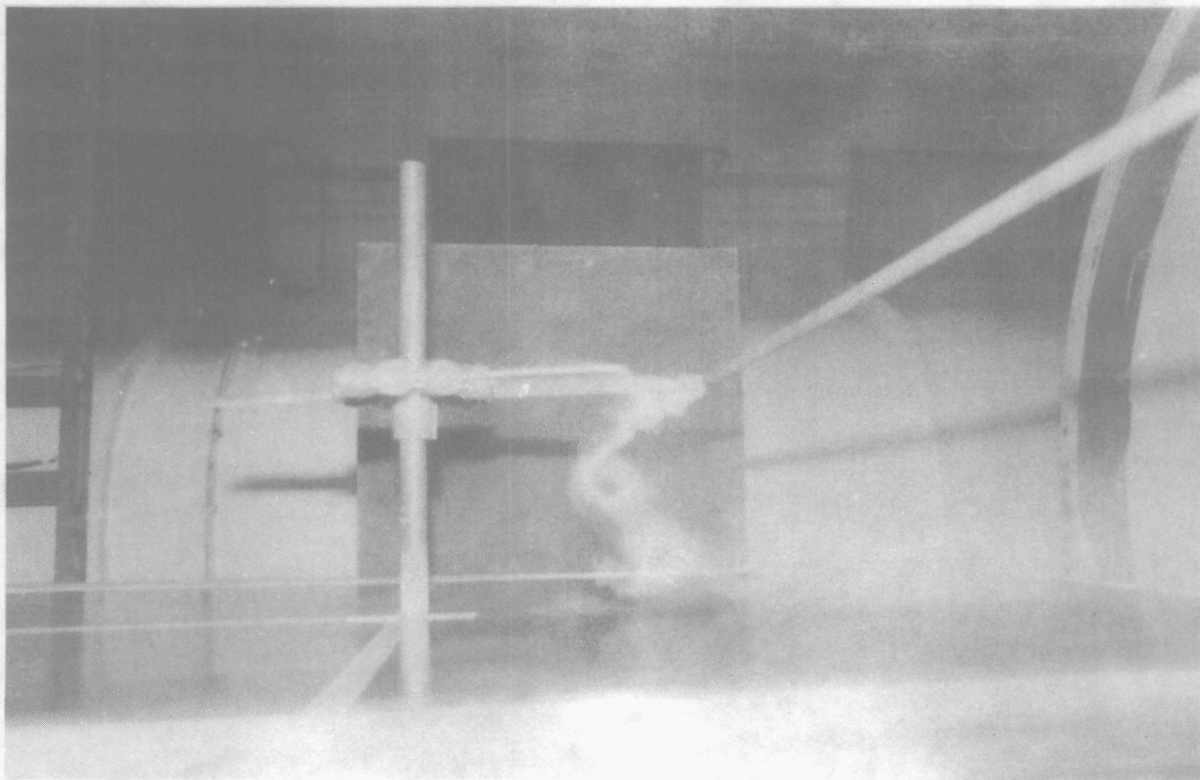
-○-○-○-○-○-  $R_e = 1.0 \times 10^5 \sim V = 24.5$  M/sec.  
 -△-△-△-△-△-  $R_e = 1.3 \times 10^5 \sim V = 30.5$  M/sec.

Fig 7 Section lift characteristic



$Z/D = 0.3$

Figure 8. Smoke Visualization of two-bladed rotor wake with  $\theta = 10^\circ$ ,  $\gamma = 0^\circ$  and  $\mu = 0$



$Z/D = 0.5$

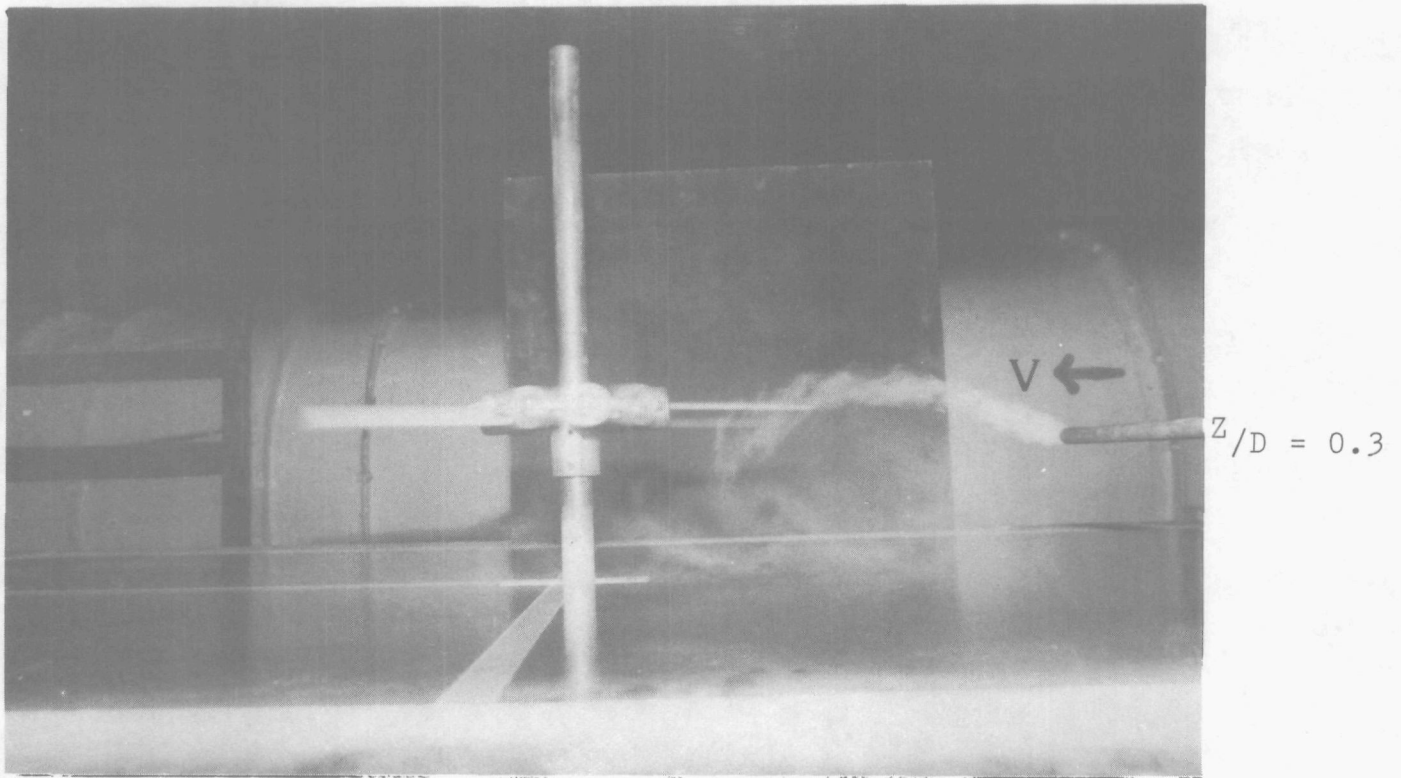
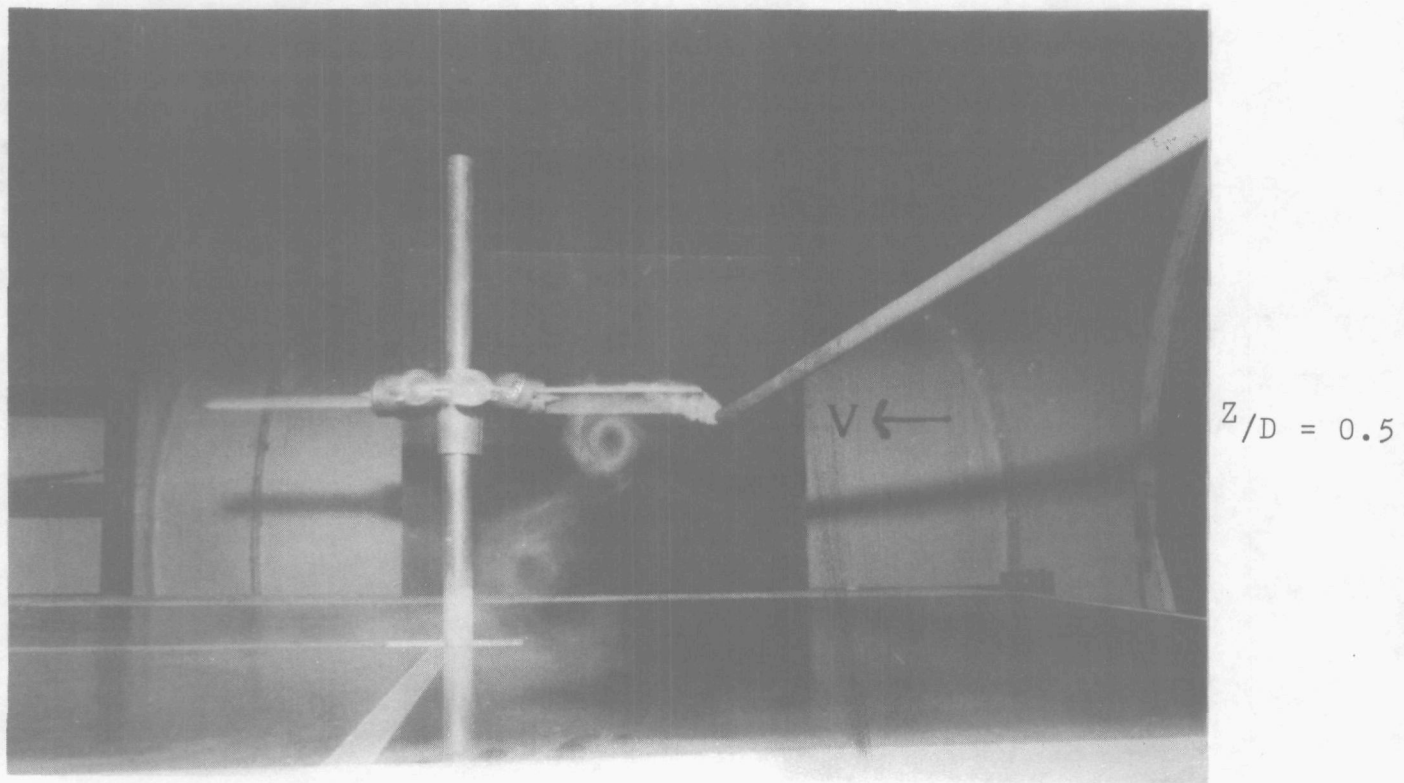
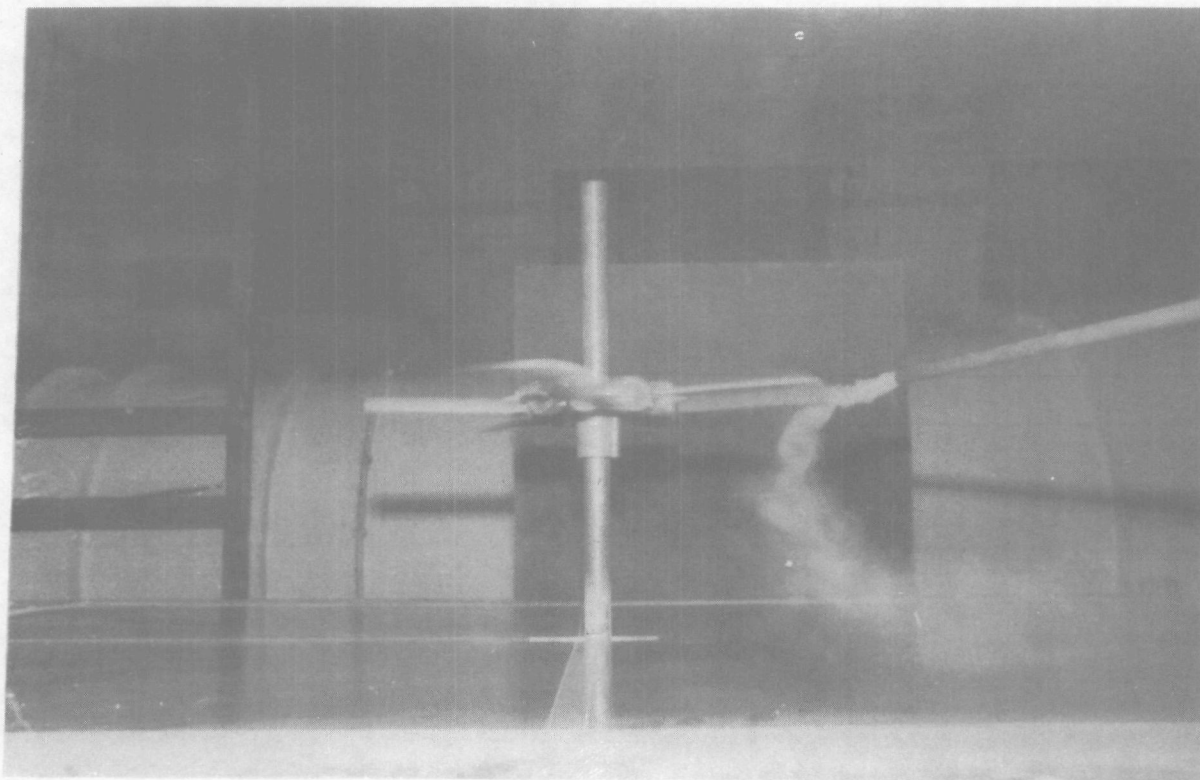


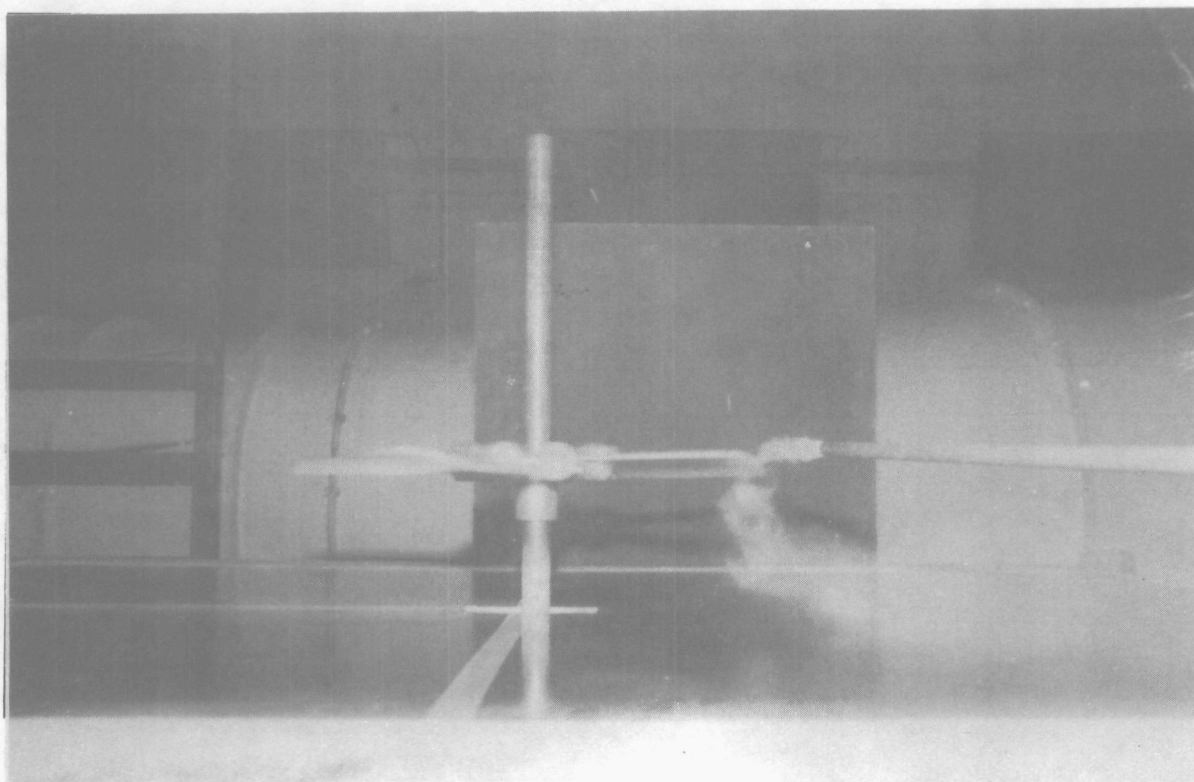
Figure 9. Smoke visualization of two-bladed rotor wake with  $\theta = 10^\circ$ ,  $\gamma = 0^\circ$  and  $\mu = 0.1$





$Z/D = 0.5$

Figure 10. Smoke visualization of five-bladed rotor wake with  $\theta = 10^\circ$ ,  $\gamma = 0^\circ$ ,  $\mu = 0$



$Z/D = 0.3$

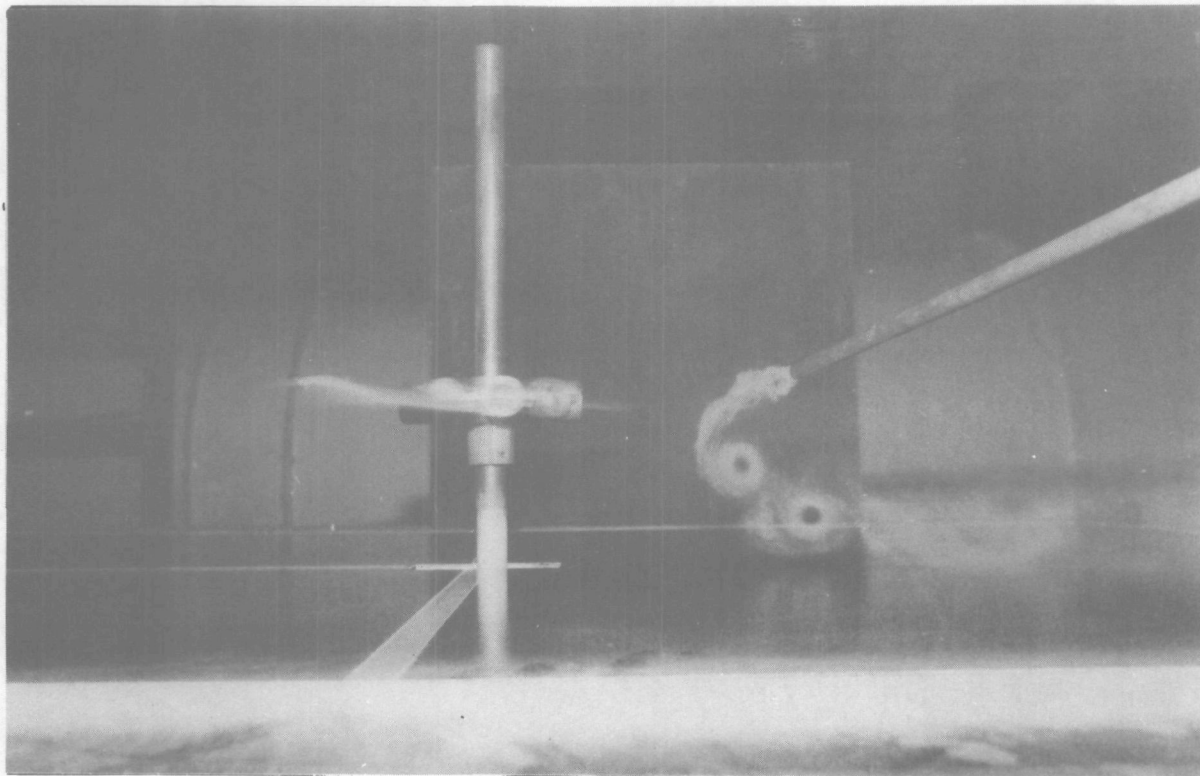
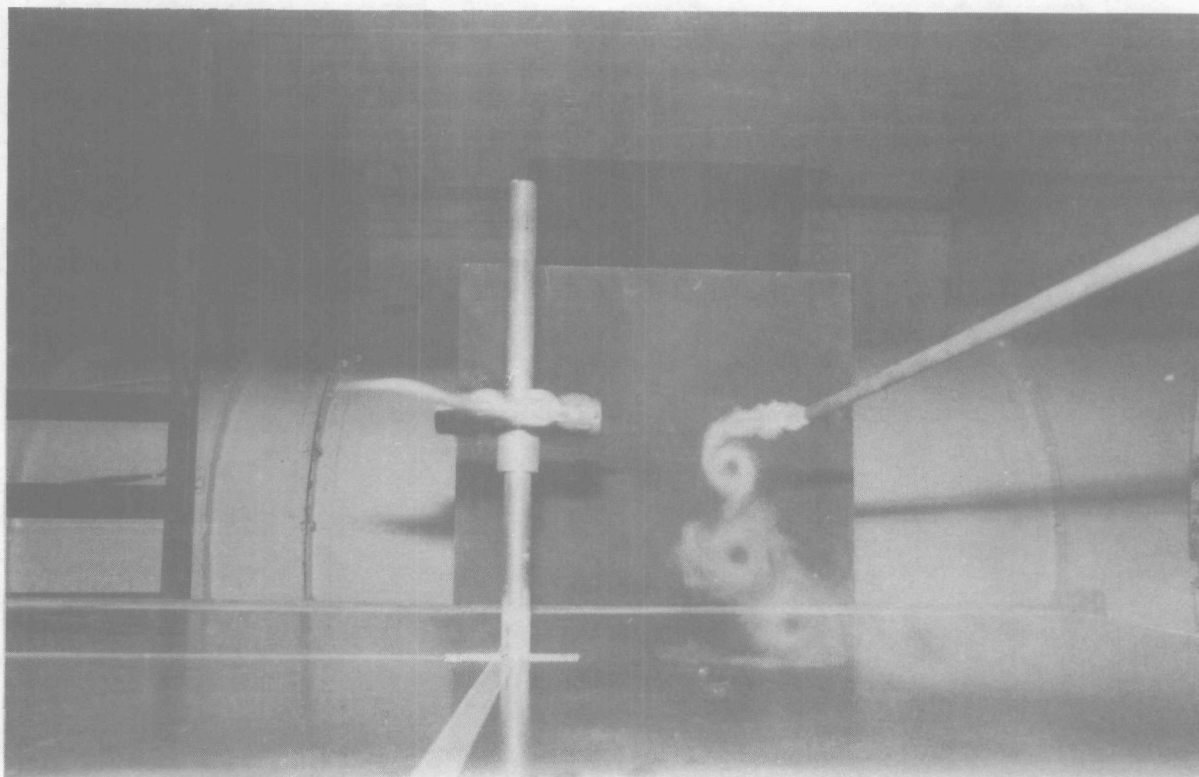


Figure 11. Smoke visualization of two-bladed rotor wake with  $\theta = 10^\circ$ ,  $\gamma = 0^\circ$ ,  $\mu = 0$  at an azimuth angle  $> 90^\circ$



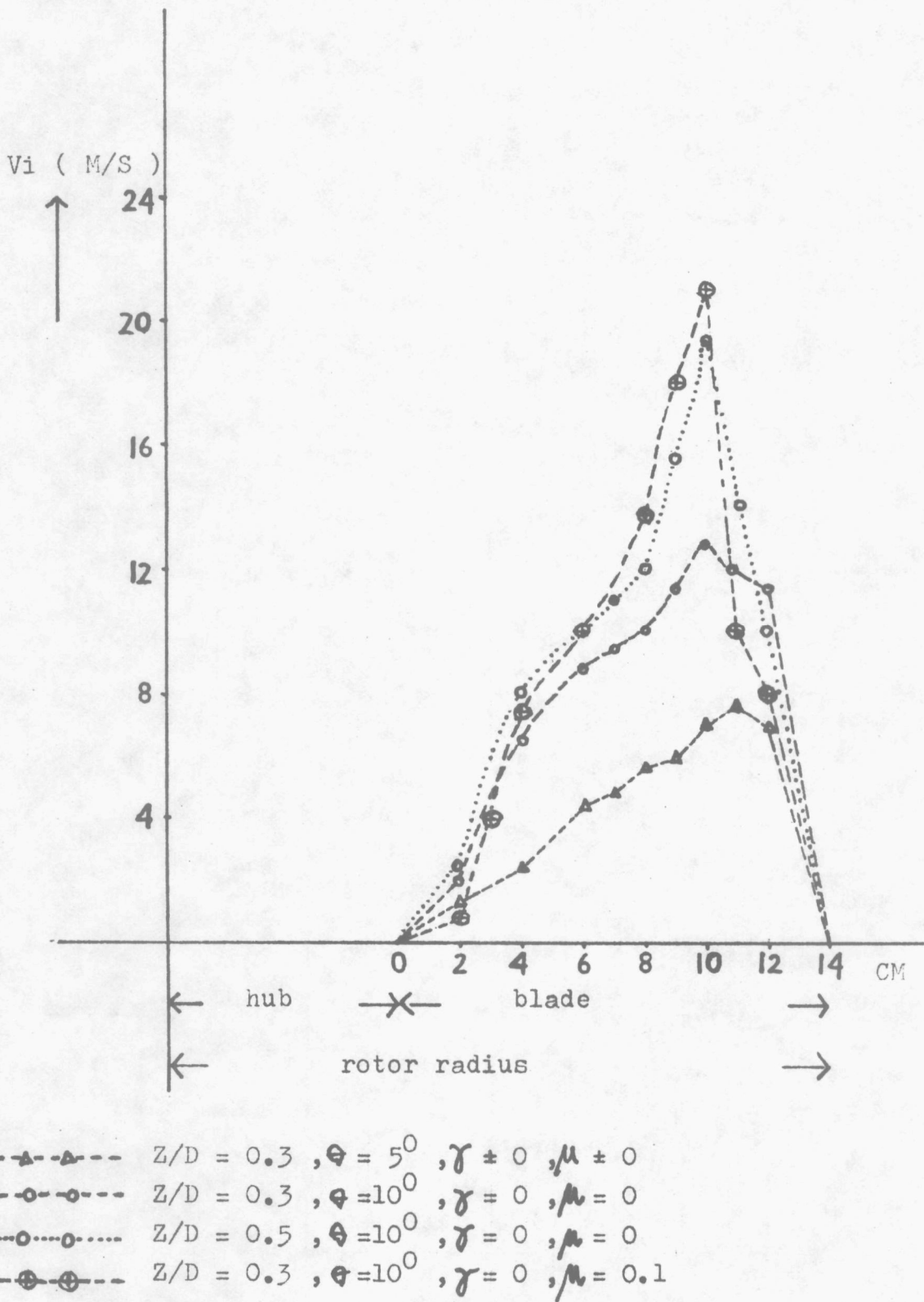


Fig 12 Vertical velocity through the disc of two bladed rotor .

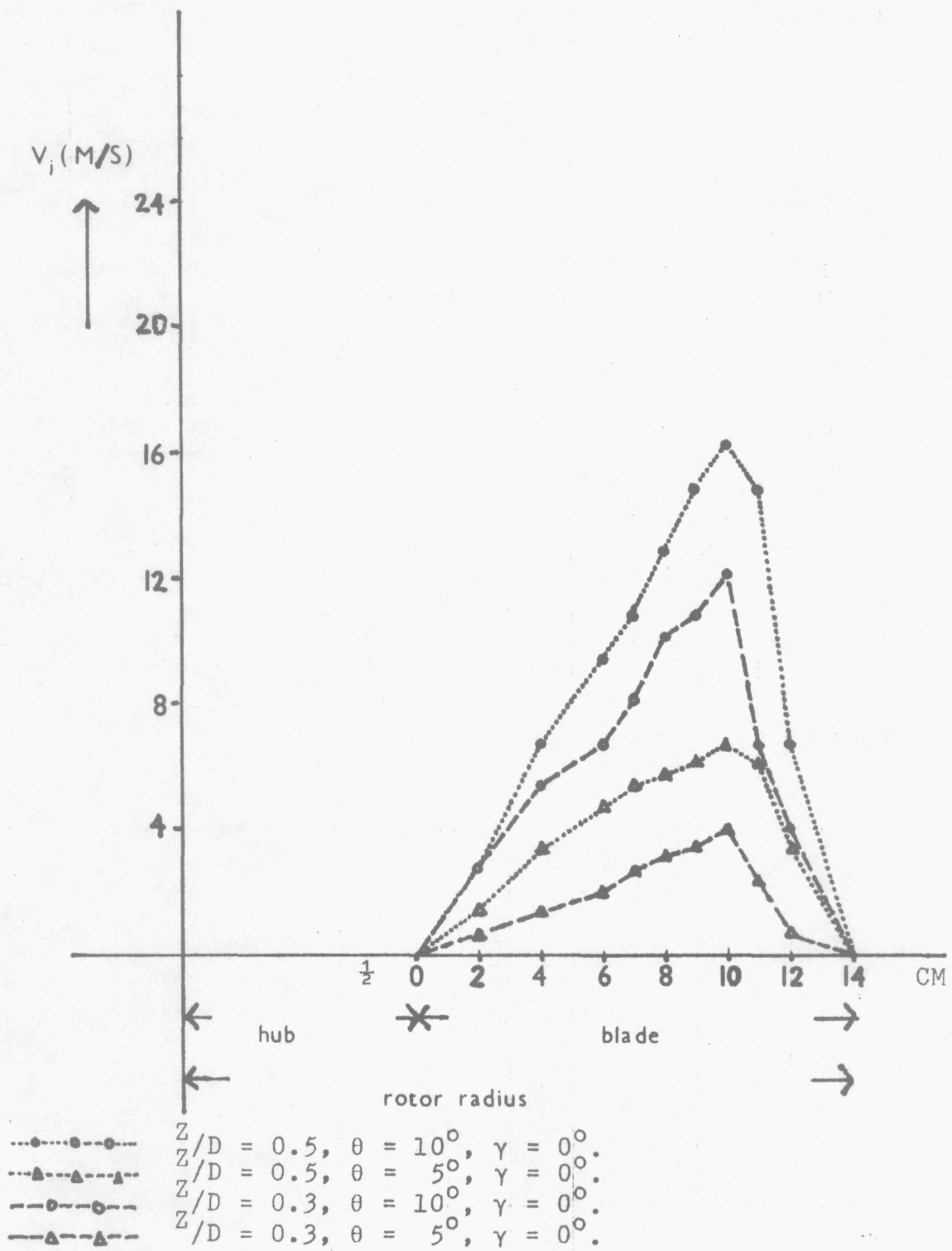


Figure 13. Vertical velocity through the disc of five-bladed rotor in no-wind condition.

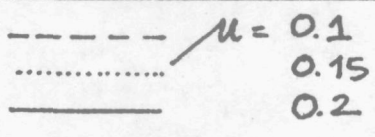
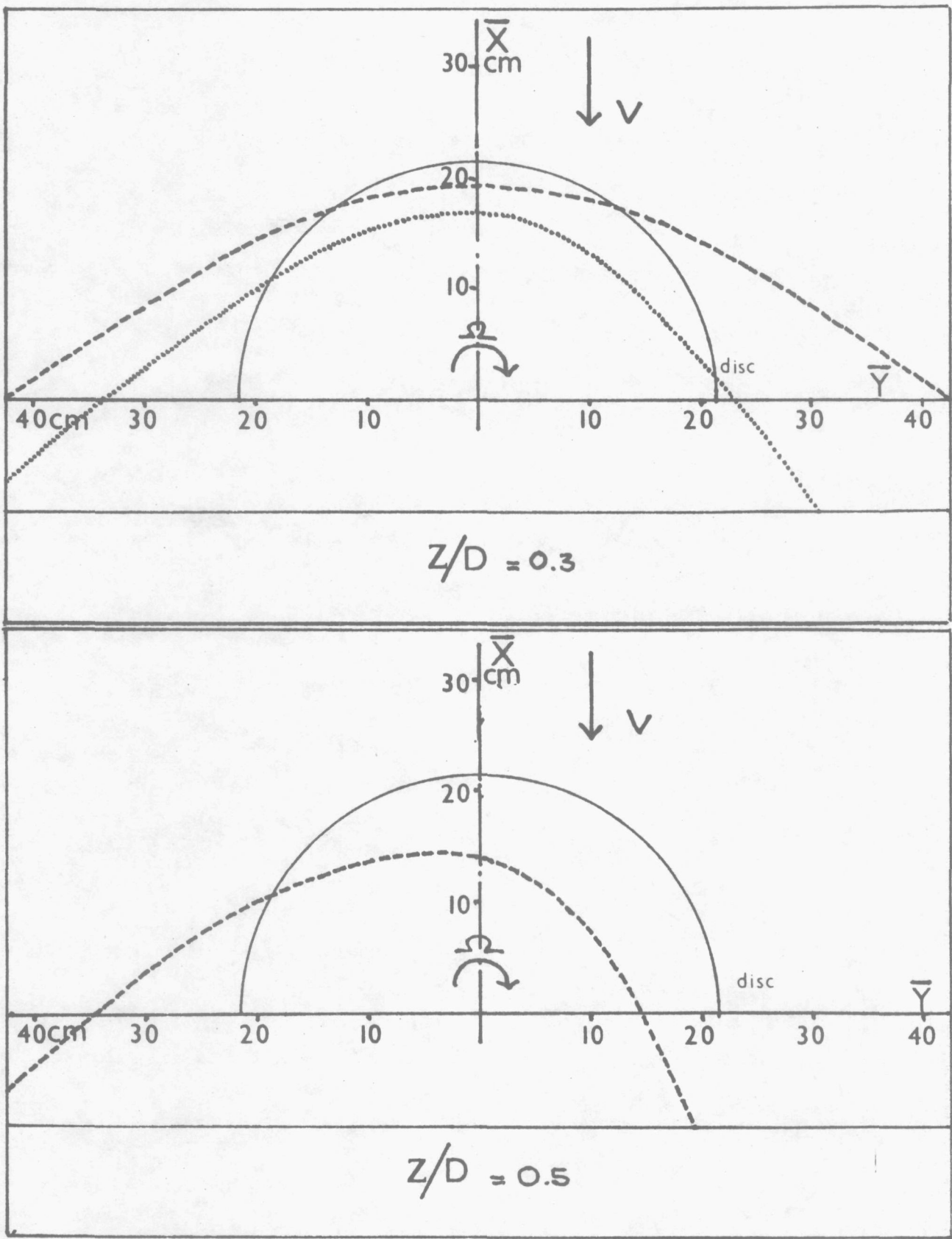
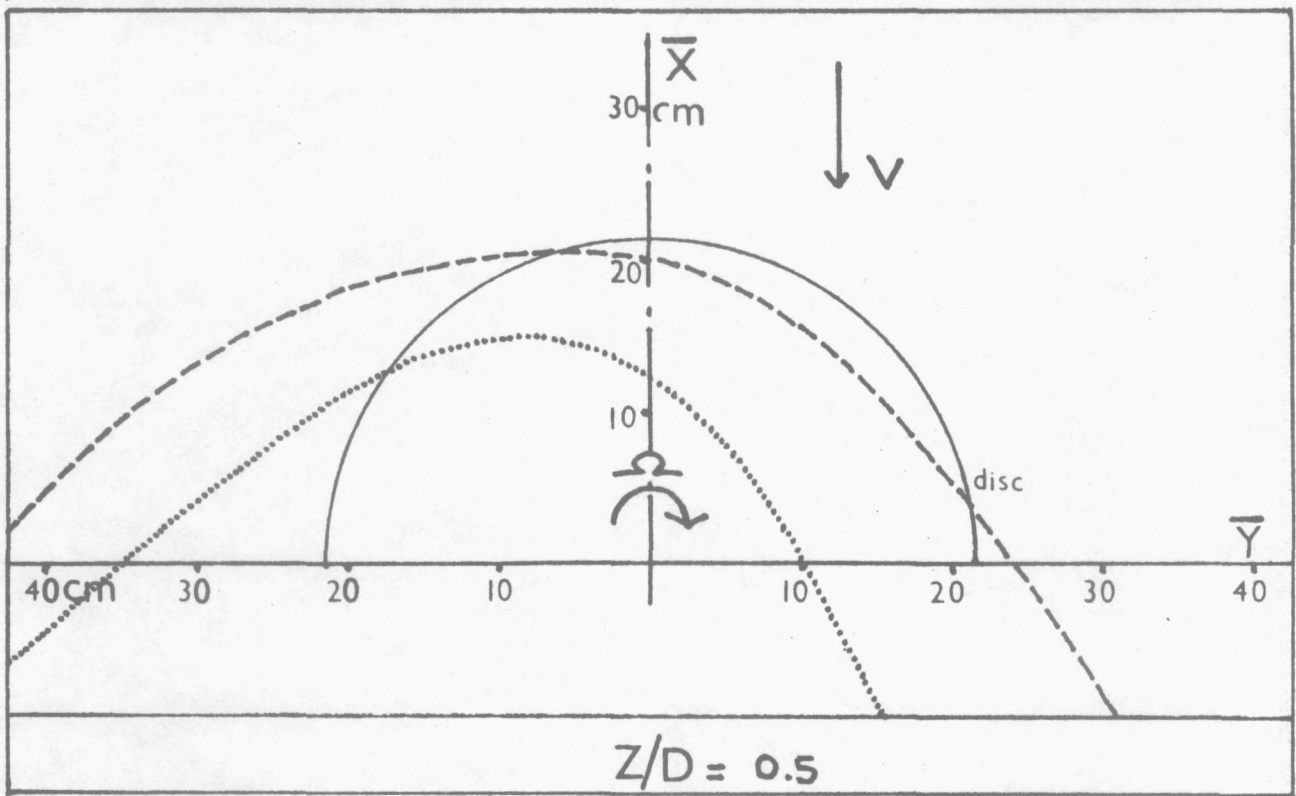
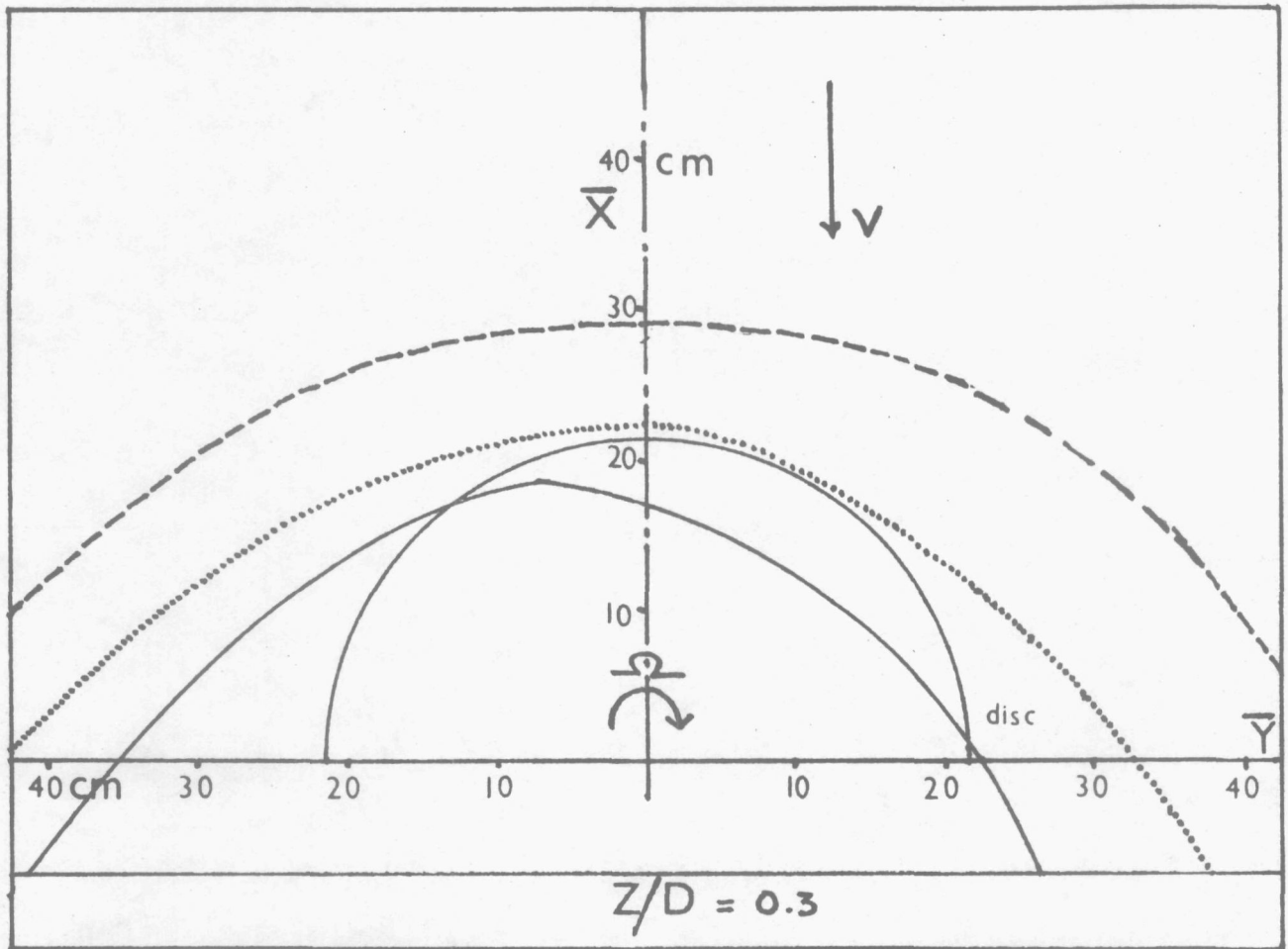
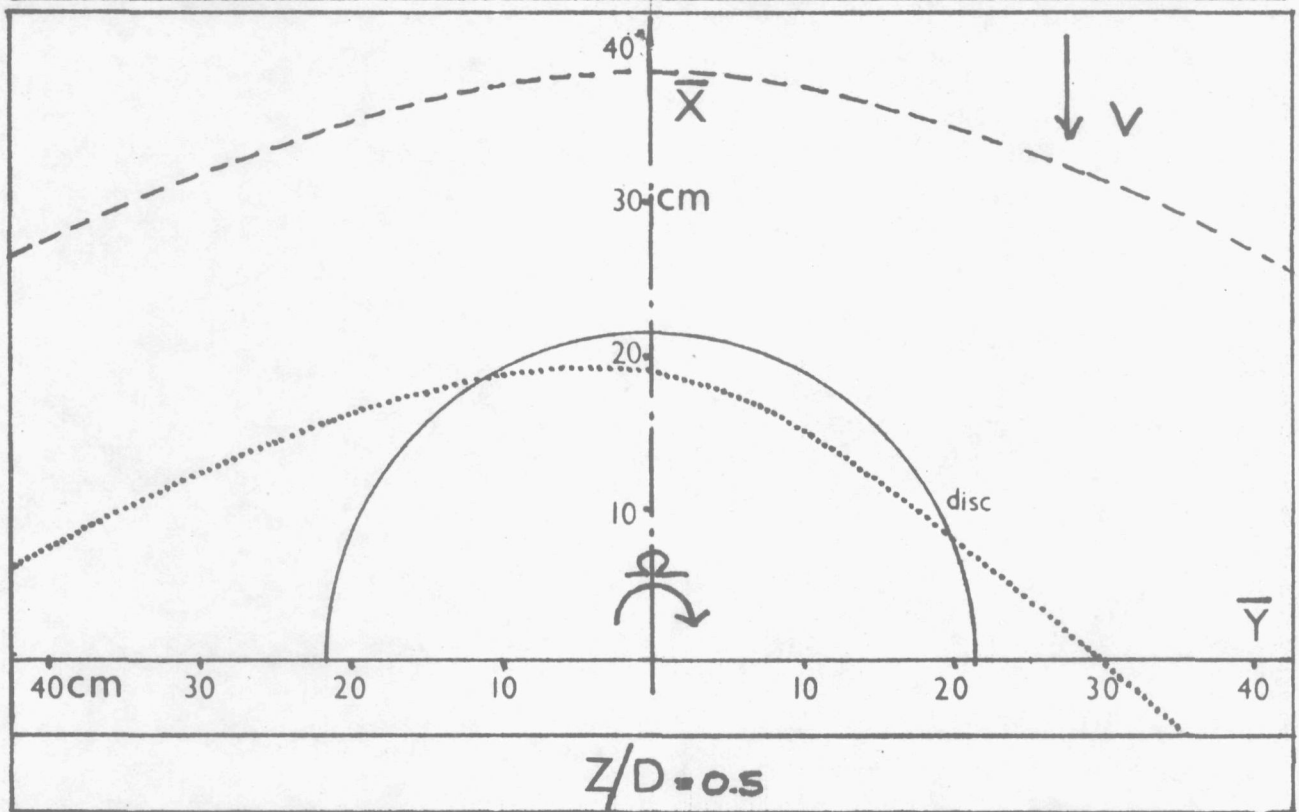
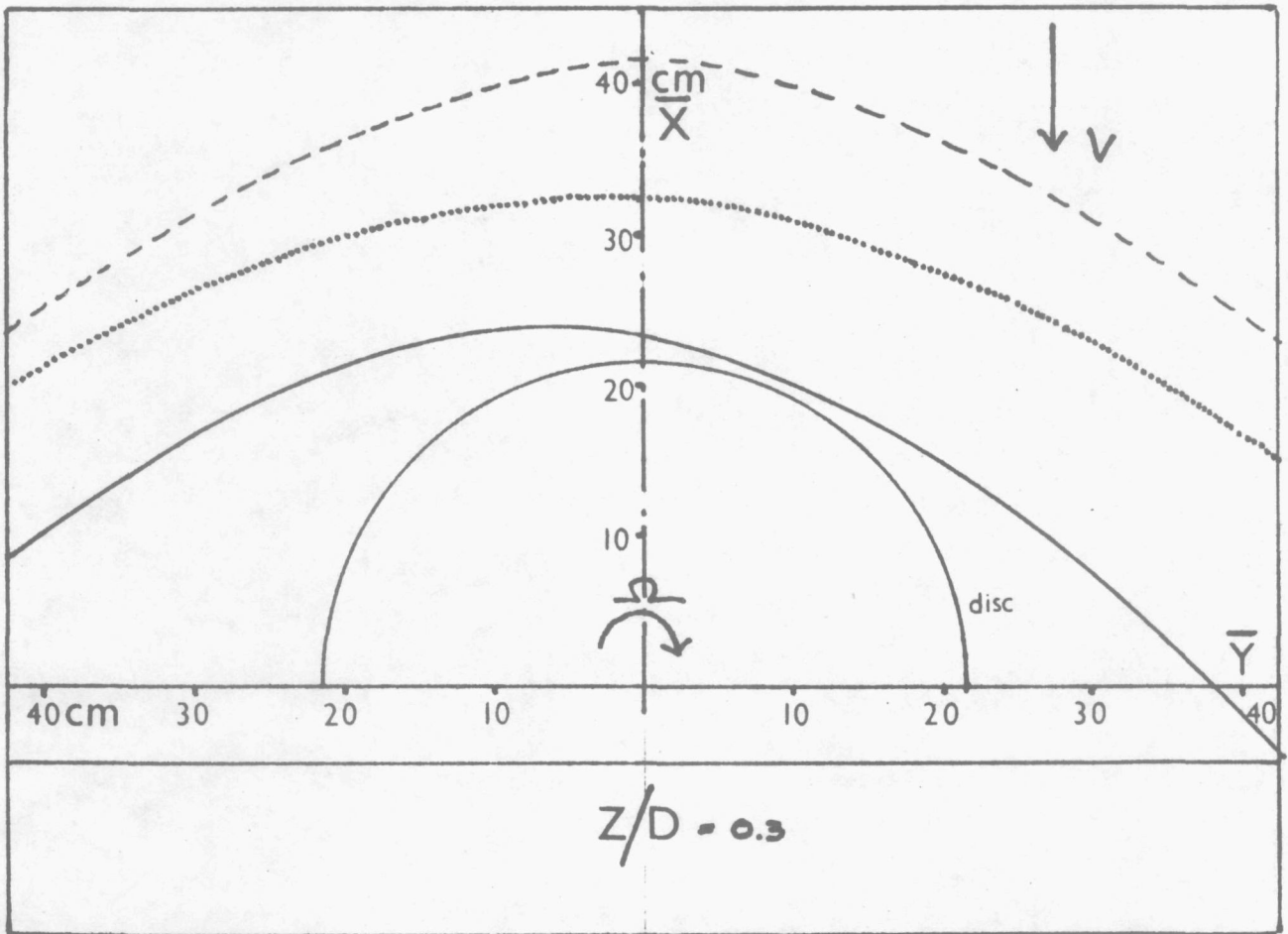


Figure 14. Surface flow visualization of two-bladed rotor with  $\theta = 5^\circ$ ,  $\gamma = 0^\circ$



- - - - -  $u = 0.1$   
 .....  $0.2$   
 \_\_\_\_\_  $0.3$

Figure 15. Flow visualization of two-bladed rotor with  $\theta = 10^\circ$ ,  $\gamma = 0^\circ$



- - - - -  $\mu = 0.1$   
 ······  $0.15$   
 —————  $0.2$

Figure 16. Surface flow visualization of five-bladed rotor with  $\theta = 10^\circ$ ,  $\gamma = 0^\circ$

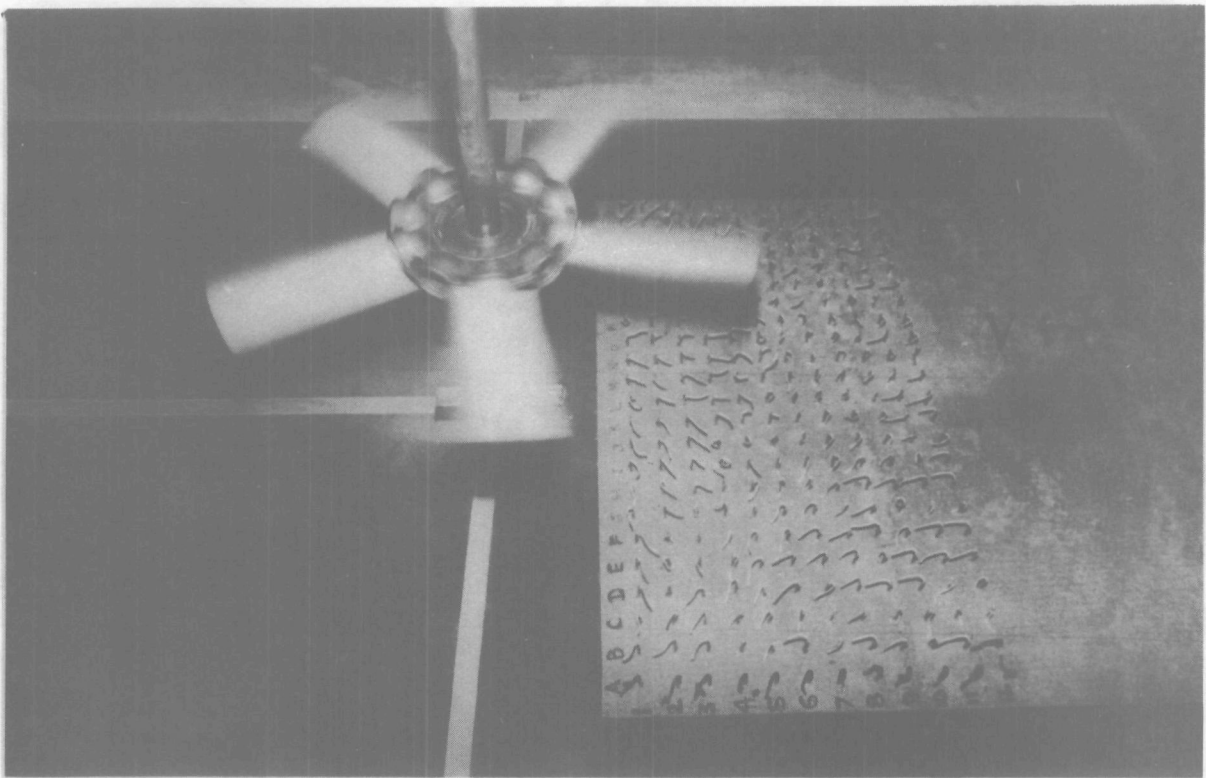


Figure 17a. Near-ground tuft grid configuration

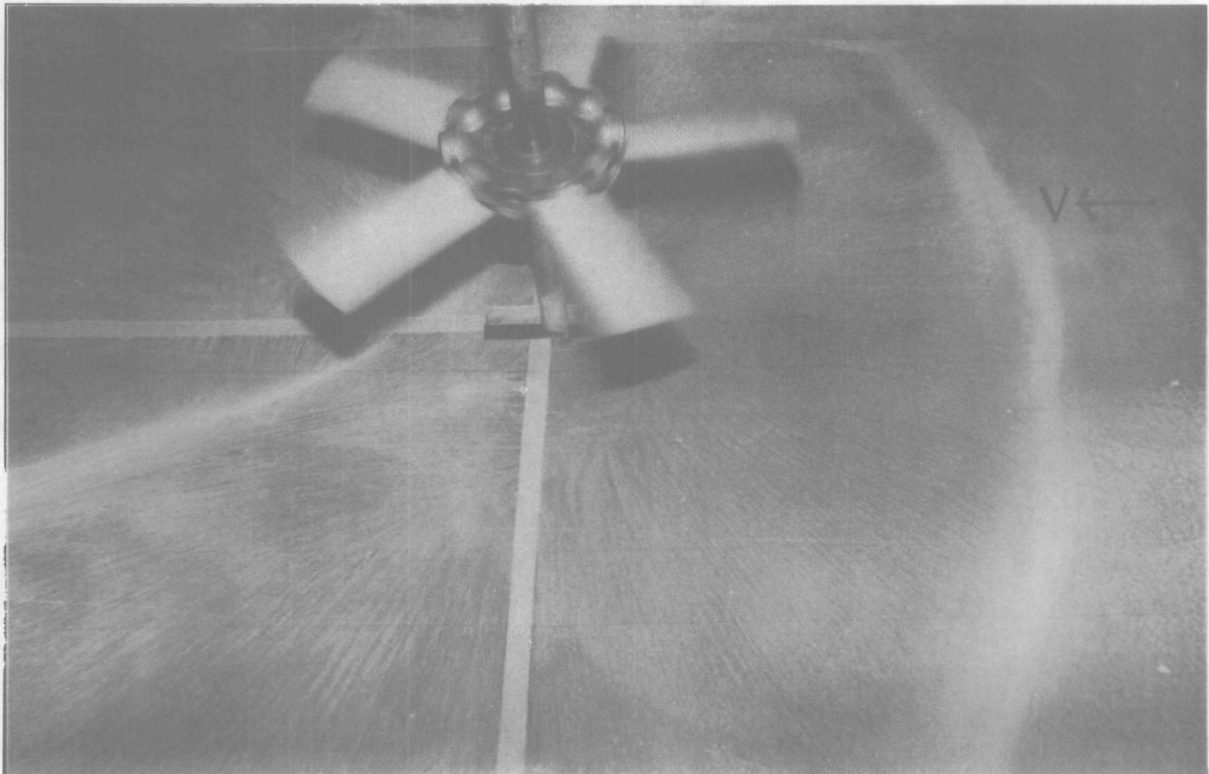


Figure 17b. Surface flow visualization

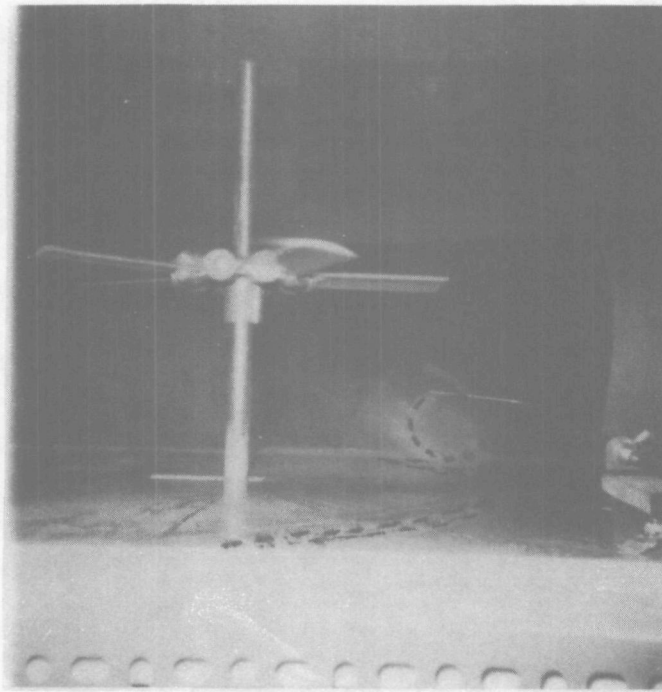


Figure 18a. Front wake ground vortex smoke visualization

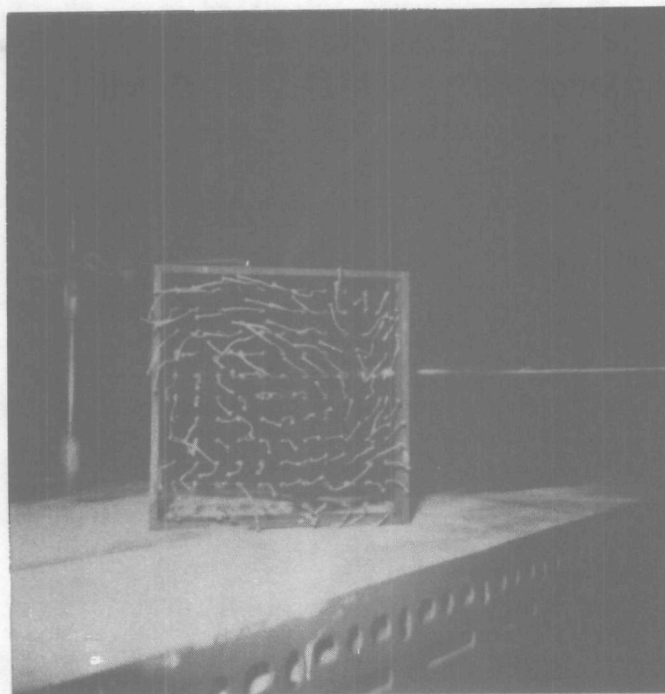


Figure 18b. Downstream wake ground vortex tuft  
grid configuration

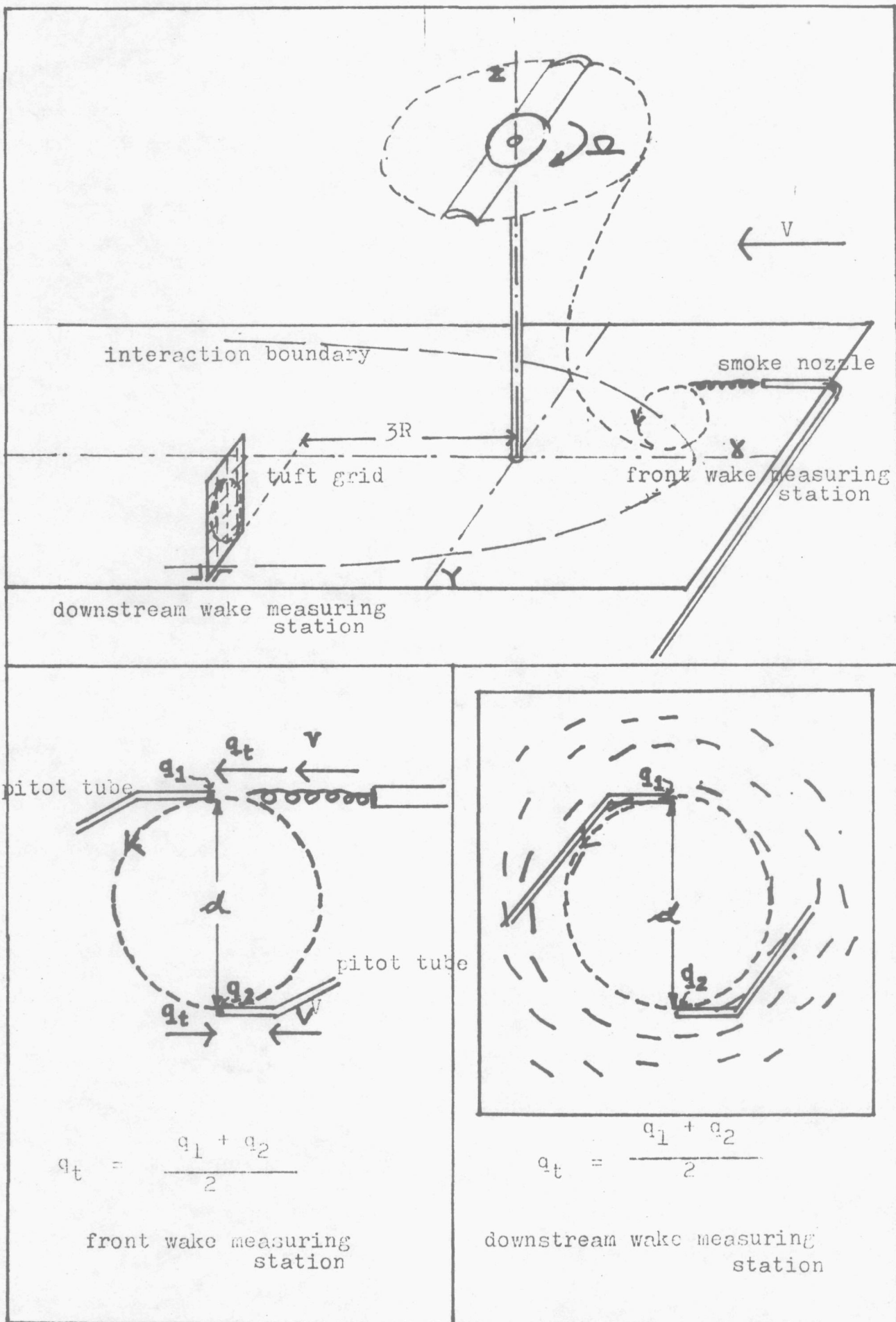


Fig 19 Measurement of ground vortex's tangential velocity .